Computers and Mathematics with Applications 160 (2024) 30–45

Contents lists available at ScienceDirect

Computers and Mathematics with Applications

journal homepage: www.elsevier.com/locate/camwa

Continuous data assimilation of a discretized barotropic vorticity model of geophysical flow

Mine Akbas [a], Amanda E. Diegel [b,1], Leo G. Rebholz [c,*,2]

[a] Tarsus University, Department of Engineering Fundamental Sciences, Faculty of Engineering, Tarsus, 81620, Mersin, Turkey
[b] Department of Mathematics and Statistics, Mississippi State University, Mississippi State, MS 39762, United States of America
[c] School of Mathematical and Statistical Sciences, Clemson University, Clemson, SC, 29364, United States of America

ARTICLE INFO

Keywords:
Barotropic vorticity equation
Quasi-geostrophic equation
Continuous data assimilation
Long time accuracy
Finite element method

ABSTRACT

We consider continuous data assimilation applied to a finite element spatial discretization and backward difference temporal discretization of the barotropic vorticity model of geophysical flow. We prove that with sufficient measurement data and properly chosen nudging parameter (guided by our analysis), the proposed algorithm achieves optimal long-time accuracy for any initial condition. While our analysis requires nudging of both the streamfunction and vorticity, our numerical tests indicate that nudging only the streamfunction can be sufficient.

1. Introduction

In this paper, we consider a numerical method that incorporates continuous data assimilation (CDA) in order to achieve long-time stable and accurate approximations to the barotropic vorticity (BV) model of geophysical flows. Geophysical flow simulations are used in the study of climate change, weather and ocean forecasting, pollutant transport in the ocean, and many other applications [46,36,24,49,13,8,48]. The BV model is one of the simplest models that can be used to represent meso and large scale geophysical flows, and is commonly used in oceanography to study midlatitude ocean circulation, but can also be extended to describe the vertical motions in the ocean [38].

The BV system, in dimensionless form, is given by [28,47]:

$$R_0 \frac{\partial \omega}{\partial t} + R_0 J(\psi, \omega) - \frac{\partial \psi}{\partial x} - \left(\frac{\delta_M}{L}\right)^3 \Delta \omega = F, \quad \text{in } (0,T]\times\Omega, \tag{1.1a}$$

$$-\Delta \psi = \omega, \quad \text{in } (0,T]\times\Omega, \tag{1.1b}$$

where ω represents vorticity, ψ represents the streamfunction,

$$J(\psi,\omega) = \frac{\partial \psi}{\partial x}\frac{\partial \omega}{\partial y} - \frac{\partial \psi}{\partial y}\frac{\partial \omega}{\partial x}$$

is the Jacobian, L is a horizontal length scale typically corresponding to a basin dimension, $R_0 > 0$ is the Rossby number describing the relationship of the fluid velocity to the length scale L, $\delta_M > 0$ is the Munk scale describing the relationship of the fluid viscosity to the length scale L, and F is the forcing term. See the paper by San, Staples, Wang, and Iliescu [47] for more details regarding the Rossby number and the Munk scale, including their derivations. Additionally, we consider appropriate initial conditions and homogeneous Dirichlet boundary condition for both the vorticity and streamfunction. These boundary conditions correspond to slip boundary conditions for the velocity and an impermeability boundary condition, respectively, in the case that the model is used to describe large scale ocean circulation [47].

* Corresponding author.
E-mail addresses: mineakbas@tarsus.edu.tr (M. Akbas), adiegel@math.msstate.edu (A.E. Diegel), rebholz@clemson.edu (L.G. Rebholz).
[1] Partially supported by NSF grant DMS 2110768.
[2] Partially supported by NSF grant DMS 2152623.

https://doi.org/10.1016/j.camwa.2024.02.004
Received 16 March 2023; Received in revised form 10 November 2023; Accepted 2 February 2024
Available online 14 February 2024

We consider herein the BV model enhanced with continuous data assimilation (CDA). While there are many types of data assimilation, CDA is very interesting because it has a solid mathematical foundation. It was developed by Azouani, Olson, and Titi in 2014 [4], and since then it has been successfully used on a wide variety of problems including Navier-Stokes equations and turbulence [4,35,18], (Rayleigh-) Bénard convection [16,14,3,1,15], a planetary geostrophic model [17] and other geophysics models [32,31], the Cahn-Hilliard equation [12], and many others. CDA has gained immense interest since its development, which has led to many improvements and uses for it, including for parameter recovery (see e.g. [9,37,43,10,34] and references therein), sensitivity analyses [11], how to nudge only some of the unknowns [1,15], numerical analyses [29,33,45,12,21], and efficient nudging methods [6,45], to name a few.

The general idea of CDA is as follows: Suppose we are given a PDE that is the correct model for the evolution of a particular physical (or other) phenomenon, with solution $u(x,t)$:

$$\begin{aligned} u_t + G(u) &= f, \\ u(x,t)|_{\partial\Omega} &= 0, \\ u(x,0) &= u_0(x). \end{aligned}$$

If the true solution is known at certain points from measurements or observables, then $I_H(u)$ is known, with I_H representing an appropriate linear interpolant. The CDA model then takes the form

$$\begin{aligned} \tilde{u}_t + G(\tilde{u}) + \mu I_H(\tilde{u} - u) &= f, \\ \tilde{u}(x,t)|_{\partial\Omega} &= 0, \\ \tilde{u}(x,0) &= \tilde{u}_0(x), \end{aligned}$$

where $\mu > 0$ is a user selected nudging parameter and $\tilde{u}_0$ is an approximated initial condition. For many such systems, given enough measurement values, it can be proven that $\|u - \tilde{u}\|_{L^2} \to 0$ exponentially fast as $t \to \infty$, regardless of how inaccurate $\tilde{u}_0$ may be as an approximation to u_0. In numerical studies with CDA, accuracy results can often avoid error growth in time since application of the Grönwall inequality can be avoided, leading to long-time optimal accuracy [21,45,20] (that is, for large enough time, the error in the computed CDA solution will be on the order of the best expected approximation error for a given spatial and temporal discretization, and will not grow with time).

To apply CDA to BV, there are two unknowns that can be nudged: the vorticity and the streamfunction. While it is likely that only measurements of the streamfunction are available in practice, we choose to nudge both the streamfunction and the vorticity here as this enables us to capture the long-time accuracy mentioned above. A model in which only the streamfunction is nudged is under current investigation and reserved as future work. The BV-CDA model thus takes the form

$$R_0 \frac{\partial \tilde{\omega}}{\partial t} + R_0 J(\tilde{\psi}, \tilde{\omega}) - \frac{\partial \tilde{\psi}}{\partial x} - \left(\frac{\delta_M}{L}\right)^3 \Delta\tilde{\omega} + \mu_1 I_H(\tilde{\omega} - \omega) = F, \quad \text{in } (0,T]\times\Omega, \tag{1.2a}$$

$$-\Delta\tilde{\psi} + \mu_2 I_H(\tilde{\psi} - \psi) = \tilde{\omega}, \quad \text{in } (0,T]\times\Omega, \tag{1.2b}$$

together with initial and boundary conditions. The purpose of this paper is to study a discretization of (1.2) that uses a backward difference temporal discretization and finite element spatial discretization. We will prove that, with CDA, solutions of the discretized system are long-time optimally accurate in time and space, and avoid Grönwall inequalities that arise in analyses of BV discretizations, e.g. [39]. Our analysis, for simplicity of exposition, is done for the case of BDF1 (backward Euler) time stepping. However, extension to BDF2 can be done in a straightforward manner utilizing the G-norm as in e.g. [30,26].

This paper is arranged as follows. In Section 2, we introduce notation and several lemmas which will be used throughout the paper. In Section 3, we introduce the finite element CDA method for the BV model and prove existence, long-time stability, and convergence of the numerical scheme. In Section 4, we demonstrate the effectiveness of the CDA scheme with several numerical experiments and, finally, in Section 5, we make some concluding remarks.

2. Notation and preliminaries

We consider a bounded open polygonal domain $\Omega \subset \mathbb{R}^2$ and define $X = H_0^1(\Omega)$ to be the subspace of $H^1(\Omega)$ with homogeneous Dirichlet boundary condition (in the trace sense). Additionally, we denote the $L^2(\Omega)$ inner product and norm by $(\cdot,\cdot)$, and $\|\cdot\|_{L^2}$, respectively, and the $H^k(\Omega)$ norm by $\|\cdot\|_{H^k}$.

We define the trilinear operator $b : X \times X \times X \to \mathbb{R}$ by

$$b(u,v,w) = (J(u,v), w), \tag{2.1}$$

and note the well-known skew-symmetric properties [19]: for $u, v \in X$,

$$b(u,v,v) = 0, \text{ and } b(u,v,u) = 0.$$

We remark that for all $v \in X$, we have the following Poincaré inequality: There exists a constant C_P depending only on Ω such that

$$\|v\|_{L^2} \le C_P \|\nabla v\|_{L^2}. \tag{2.2}$$

Additionally, the following lemmas will be useful throughout the remainder of the paper.

Lemma 2.1. *Suppose the constants r and B satisfy $r > 1$ and $B \ge 0$. Then if the sequence of real numbers $\{a_m\}$ satisfies*

$$r a_{m+1} \le a_m + B, \tag{2.3}$$

we have that

$$a_{m+1} \leq a_0 \left(\frac{1}{r}\right)^{m+1} + \frac{B}{r-1}.$$

Proof. See [33]. □

2.1. Numerical preliminaries

For the numerical method, we take a regular conforming triangulation of Ω, denoted by τ_h. For a positive integer r, we define the continuous finite element space with rth degree polynomials on each element K of the triangulation as $\mathcal{M}_r^h := \{v \in C(\overline{\Omega}) |\ v_K = v|_K \in \mathcal{P}_r(\Omega)\ \forall K \in \tau_h\} \subset H^1(\Omega)$. Then, for a given positive integer k, we define the finite element space $Y_h := \mathcal{M}_k^h$. Additionally, we define a subset of Y_h as $X_h := Y_h \cap H_0^1(\Omega)$.

The trilinear operator has skew-symmetric properties on the finite element spaces as demonstrated by Fix in [19]. We state these properties here and note that the proofs follow by integration by parts and the divergence theorem.

Lemma 2.2. *For $\psi, \xi \in X_h$ and $\chi \in Y_h$,*

$$b(\psi, \xi, \xi) = 0 \quad \text{and} \quad b(\psi, \chi, \psi) = 0.$$

Proof. See [19]. □

We define the discrete Laplacian operator $\Delta_h : X \to X_h$ in the usual way by

$$\left(\Delta_h \psi, \chi\right) = -\left(\nabla \psi, \nabla \chi\right) \quad \forall \chi \in X_h, \tag{2.4}$$

and additionally define I_H to be an interpolation operator that satisfies: For a given mesh τ_H with $H \leq 1$ and associated finite element space Y_H,

$$\left\| I_H(w) - w \right\|_{L^2} \leq C_I H \left\| \nabla w \right\|_{L^2}, \tag{2.5}$$

$$\left\| I_H(w) \right\|_{L^2} \leq C_I \left\| w \right\|_{L^2}, \tag{2.6}$$

where $C_I > 0$ is independent of w, for any $w \in H_0^1(\Omega)$. Examples of such I_H are the L^2 projection onto Y_H, where Y_H consists of piecewise constants over τ_H, and the Scott-Zhang interpolant [22].

Finally, we will utilize the following properties of the H^1 projection operator into the finite element space X_h, denoted by $R_h : X \to X_h$, in the convergence analysis:

Lemma 2.3. *Given $\psi \in H^{k+1}(\Omega)$, the following estimates are satisfied [7]:*

1. $\|\psi - R_h(\psi)\|_{L^2} \leq C h^{k+1} \|\psi\|_{H^{k+1}}$,
2. $\|\nabla(\psi - R_h(\psi))\|_{L^2} \leq C h^{k} \|\psi\|_{H^{k+1}}$.

3. A numerical scheme for BV with CDA

We now present and analyze a discretization of (1.2) which utilizes backward Euler time stepping and a finite element spatial discretization. Specifically, we consider a uniform partition of time such that $t_m = m\Delta t$ where the time step size is $\Delta t := t_{i+1} - t_i$ for $i = 0, 1, 2, \cdots$.

Algorithm 3.1. *Let $\omega^{m+1} := \omega(t_{m+1})$ and $\psi^{m+1} := \psi(t_{m+1})$ be the solution to the BV system (1.1) at time t_{m+1} and let the forcing term at time t_{m+1}, denoted by $F^{m+1} := F(t_{m+1})$, be given. Given $\omega_h^0 \in X_h$, find $\omega_h^{m+1} \in X_h$ and $\psi_h^{m+1} \in X_h$, for $m = 0, 1, 2, 3, \ldots$ satisfying*

$$R_0\left(\frac{\omega_h^{m+1} - \omega_h^m}{\Delta t}, v_h\right) + R_0 b(\psi_h^{m+1}, \omega_h^{m+1}, v_h) - \left(\frac{\partial \psi_h^{m+1}}{\partial x}, v_h\right) + \left(\frac{\delta_M}{L}\right)^3 \left(\nabla \omega_h^{m+1}, \nabla v_h\right) + \mu_1 (I_H(\omega_h^{m+1} - \omega^{m+1}), v_h) = (F^{m+1}, v_h), \tag{3.1}$$

$$\left(\nabla \psi_h^{m+1}, \nabla \chi_h\right) + \mu_2 (I_H(\psi_h^{m+1} - \psi^{m+1}), \chi_h) = (\omega_h^{m+1}, \chi_h), \tag{3.2}$$

for every $v_h, \chi_h \in X_h$.

Changing the nudging terms to instead be of the form $(I_H(\omega_h^{m+1} - \omega^{m+1}), I_H v_h)$ (as proposed in [45]) would be equivalent if I_H is chosen to be an L^2 projection operator onto a finite element space. Whether it makes sense to alter the nudging terms depends on the interpolation operator chosen and how to most efficiently implement it, and it is advantageous to make such a change in the case of algebraic nudging [45]. For some PDEs, it can even reduce restrictions on the nudging parameter [20]. All the results herein will still hold (up to changes in constants) with the alternative nudging formulation, although more analysis is required to achieve these results.

3.1. Well-posedness

Proving well-posedness of Algorithm 3.1 is a challenging task. The problem reduces immediately to proving well-posedness of the algorithm at an individual time step. Below we give partial results. We prove existence under the assumption of a particular interpolation operator I_H and also under the assumption that $X_H \subset X_h$. Although we believe that existence will hold in a more general setting, proving such a statement appears to be quite difficult. For uniqueness, a CFL condition arises, which is not unexpected. In the case of steady nonlinear PDEs for fluids, often small data

conditions are required for uniqueness proofs [5,23]. In our setting, instead of using a small data condition, we use the time derivative term with coefficient $\frac{1}{\Delta t}$ to absorb the right hand side terms after applying the inverse inequality to them; here, Δt sufficiently small allows for uniqueness.

3.1.1. Existence

Lemma 3.1. *Consider (3.1)-(3.2) for fixed m, and assume that I_H is chosen to be the L^2 projection onto $X_H \subset X_h$. Then for sufficiently small Δt, solutions exist.*

Proof. This follows as a discrete analogue to the proof of Lemma 3.2 in [5], which relies on the Leray-Schauder theorem. The main difference is the nudging terms, which do not create difficulty for this choice of I_H. □

Remark 3.1. *The existence lemma above relies on the choice of a coarse mesh interpolation operator I_H and that $X_H \subset X_h$. Outside of this setting, separate analyses would need to be performed in order to prove existence. While we expect this to still hold in general, in particular, because this is in a discrete setting where the inverse inequality can be applied, a different choice of I_H may create additional restrictions on Δt, H, μ_1 and μ_2.*

3.1.2. Long-time stability

We now prove stability of the scheme. The stability result has no condition on the time step size, but does require restrictions on H and the nudging parameters, μ_1 and μ_2.

Lemma 3.2. *Let $F \in L^\infty(0,\infty;L^2(\Omega))$ and $\omega, \psi \in L^\infty(0,\infty;L^2(\Omega))$, and initial conditions ω_h^0, ψ_h^0 be given. Assume that*

$$2(1+2C_P^2) \le \mu_1 \le \frac{(\delta_M/L)^3}{4C_I^2H^2} \quad \text{and} \quad \mu_2 \le \frac{1}{4C_I^2H^2}. \tag{3.3}$$

Then for any $\Delta t > 0$ and any integer $m \ge 0$, solutions to Algorithm 3.1 satisfy the following bounds:

$$\|\omega_h^m\|_{L^2}^2 \le \left(\frac{1}{1+\lambda^*}\right)^m \|\omega_h^0\|_{L^2}^2 + 2R_0C_P^2\,(\delta_M/L)^{-3}\,R^* =: C_\omega^2, \tag{3.4}$$

and

$$\|\nabla\psi_h^m\|_{L^2}^2 \le 2\mu_2C_I^2\|\psi\|_{L^\infty(0,\infty;L^2(\Omega))}^2 + 2\,C_P^2C_\omega,$$

where R^* and λ^* are defined

$$R^* := R_0^{-1}\left(2\mu_1C_I^2\|\omega\|_{L^\infty(0,\infty;L^2(\Omega))}^2 + C_P^2\,(\delta_M/L)^{-3}\,\|F\|_{L^\infty(0,\infty;L^2(\Omega))}^2 + 4\mu_2C_I^2\|\psi\|_{L^\infty(0,\infty;L^2(\Omega))}^2\right),$$
$$\lambda^* := \frac{(\delta_M/L)^3}{2R_0C_P^2}\Delta t.$$

Proof. Setting $v_h = \omega_h^{m+1}$ in (3.1) and $\chi_h = \psi_h^{m+1}$ in (3.2) and using the polarization identity along with Lemma 2.2, yields

$$\begin{aligned}&\frac{R_0}{2\Delta t}\left[\|\omega_h^{m+1}\|_{L^2}^2 - \|\omega_h^m\|_{L^2}^2 + \|\omega_h^{m+1}-\omega_h^m\|_{L^2}^2\right] + \left(\frac{\delta_M}{L}\right)^3\|\nabla\omega_h^{m+1}\|_{L^2}^2 + \mu_1\|\omega_h^{m+1}\|_{L^2}^2\\ &= \left(\frac{\partial\psi_h^{m+1}}{\partial x}, \omega_h^{m+1}\right) + \mu_1(I_H(\omega^{m+1}),\omega_h^{m+1}) - \mu_1(I_H(\omega_h^{m+1})-\omega_h^{m+1},\omega_h^{m+1}) + (F^{m+1},\omega_h^{m+1}),\end{aligned} \tag{3.5}$$

and

$$\|\nabla\psi_h^{m+1}\|_{L^2}^2 + \mu_2\|\psi_h^{m+1}\|_{L^2}^2 = \mu_2(I_H(\psi^{m+1}),\psi_h^{m+1}) - \mu_2(I_H(\psi_h^{m+1})-\psi_h^{m+1},\psi_h^{m+1}) + (\omega_h^{m+1},\psi_h^{m+1}). \tag{3.6}$$

Applying the Cauchy-Schwarz, Poincaré's and Young's inequalities together with the interpolation properties on the right hand sides of (3.5) and (3.6) produces

$$\begin{aligned}&\frac{R_0}{2\Delta t}\left[\|\omega_h^{m+1}\|_{L^2}^2 - \|\omega_h^m\|_{L^2}^2 + \|\omega_h^{m+1}-\omega_h^m\|_{L^2}^2\right] + \left(\frac{\delta_M}{L}\right)^3\|\nabla\omega_h^{m+1}\|_{L^2}^2 + \mu_1\|\omega_h^{m+1}\|_{L^2}^2\\ &\le \|\nabla\psi_h^{m+1}\|_{L^2}\|\omega_h^{m+1}\|_{L^2} + \mu_1C_IH\|\omega^{m+1}\|_{L^2}\|\omega_h^{m+1}\|_{L^2} + \mu_1C_IH\|\nabla\omega_h^{m+1}\|_{L^2}\|\omega_h^{m+1}\|_{L^2} + \|F^{m+1}\|_{L^2}C_P\|\nabla\omega_h^{m+1}\|_{L^2}\\ &\le \frac{1}{2}\|\nabla\psi_h^{m+1}\|_{L^2}^2 + \frac{1}{2}\|\omega_h^{m+1}\|_{L^2}^2 + \mu_1C_I^2\|\omega^{m+1}\|_{L^2}^2 + \frac{\mu_1}{4}\|\omega_h^{m+1}\|_{L^2}^2\\ &\quad + \mu_1C_I^2H^2\|\nabla\omega_h^{m+1}\|_{L^2}^2 + \frac{\mu_1}{4}\|\omega_h^{m+1}\|_{L^2}^2 + \frac{C_P^2}{2}\left(\frac{\delta_M}{L}\right)^{-3}\|F^{m+1}\|_{L^2}^2 + \frac{1}{2}\left(\frac{\delta_M}{L}\right)^3\|\nabla\omega_h^{m+1}\|_{L^2}^2,\end{aligned}$$

and

$$\begin{aligned}\|\nabla\psi_h^{m+1}\|_{L^2}^2 + \mu_2\|\psi_h^{m+1}\|_{L^2}^2 &\le \mu_2C_I\|\psi^{m+1}\|_{L^2}\|\psi_h^{m+1}\|_{L^2} + \mu_2C_IH\|\nabla\psi_h^{m+1}\|_{L^2}\|\psi_h^{m+1}\|_{L^2} + \|\omega_h^{m+1}\|_{L^2}C_P\|\nabla\psi_h^{m+1}\|_{L^2}\\ &\le \mu_2C_I^2\|\psi^{m+1}\|_{L^2}^2 + \frac{\mu_2}{4}\|\psi_h^{m+1}\|_{L^2}^2 + \mu_2C_I^2H^2\|\nabla\psi_h^{m+1}\|_{L^2}^2 + \frac{\mu_2}{4}\|\psi_h^{m+1}\|_{L^2}^2 + \frac{C_P^2}{2}\|\omega_h^{m+1}\|_{L^2}^2 + \frac{1}{2}\|\nabla\psi_h^{m+1}\|_{L^2}^2.\end{aligned}$$

Combining like terms yields

$$\frac{R_0}{2\Delta t}\left[\|\omega_h^{m+1}\|_{L^2}^2-\|\omega_h^m\|_{L^2}^2+\|\omega_h^{m+1}-\omega_h^m\|_{L^2}^2\right]+\frac{1}{2}\left(\frac{\delta_M}{L}\right)^3\left(1-2\mu_1C_I^2H^2\left(\frac{\delta_M}{L}\right)^{-3}\right)\|\nabla\omega_h^{m+1}\|_{L^2}^2+\frac{1}{2}\left(\mu_1-1\right)\|\omega_h^{m+1}\|_{L^2}^2$$
$$\leq\frac{1}{2}\|\nabla\psi_h^{m+1}\|_{L^2}^2+\mu_1C_I^2\|\omega\|_{L^\infty(0,\infty;L^2(\Omega))}^2+\frac{C_P^2}{2}\left(\frac{\delta_M}{L}\right)^{-3}\|F\|_{L^\infty(0,\infty;L^2(\Omega))}^2, \tag{3.7}$$

and

$$\frac{1}{2}\left(1-2\mu_2C_I^2H^2\right)\|\nabla\psi_h^{m+1}\|_{L^2}^2+\frac{\mu_2}{2}\|\psi_h^{m+1}\|_{L^2}^2\leq\mu_2C_I^2\|\psi\|_{L^\infty(0,\infty;L^2(\Omega))}^2+\frac{C_P^2}{2}\|\omega_h^{m+1}\|_{L^2}^2. \tag{3.8}$$

Applying (3.3) on the left hand side of (3.8), multiplying by 4, and dropping the second left hand side term, we obtain

$$\|\nabla\psi_h^{m+1}\|_{L^2}^2\leq4\mu_2C_I^2\|\psi\|_{L^\infty(0,\infty;L^2(\Omega))}^2+2C_P^2\|\omega_h^{m+1}\|_{L^2}^2. \tag{3.9}$$

Inserting this bound on the right hand side of (3.7), rearranging terms produces

$$\frac{R_0}{2\Delta t}\left[\|\omega_h^{m+1}\|_{L^2}^2-\|\omega_h^m\|_{L^2}^2+\|\omega_h^{m+1}-\omega_h^m\|_{L^2}^2\right]+\frac{1}{2}\left(\frac{\delta_M}{L}\right)^3\left(1-2\mu_1C_I^2H^2\left(\frac{\delta_M}{L}\right)^{-3}\right)\|\nabla\omega_h^{m+1}\|_{L^2}^2+\frac{1}{2}\left(\mu_1-(1+2C_P^2)\right)\|\omega_h^{m+1}\|_{L^2}^2$$
$$\leq\mu_1C_I^2\|\omega\|_{L^\infty(0,\infty;L^2(\Omega))}^2+\frac{C_P^2}{2}\left(\frac{\delta_M}{L}\right)^{-3}\|F\|_{L^\infty(0,\infty;L^2(\Omega))}^2+2\mu_2C_I^2\|\psi\|_{L^\infty(0,\infty;L^2(\Omega))}^2. \tag{3.10}$$

Using (3.3) and multiplying the resulting inequality by $\frac{2\Delta t}{R_0}$ yields

$$\|\omega_h^{m+1}\|_{L^2}^2-\|\omega_h^m\|_{L^2}^2+\|\omega_h^{m+1}-\omega_h^m\|_{L^2}^2+\frac{(\delta_M/L)^3}{2R_0}\Delta t\,\|\nabla\omega_h^{m+1}\|_{L^2}^2+\frac{\mu_1\Delta t}{4R_0}\|\omega_h^{m+1}\|_{L^2}^2$$
$$\leq R_0^{-1}\Delta t\left(2\mu_1C_I^2\|\omega\|_{L^\infty(0,\infty;L^2(\Omega))}^2+C_P^2\,(\delta_M/L)^{-3}\,\|F\|_{L^\infty(0,\infty;L^2(\Omega))}^2+4\mu_2C_I^2\|\psi\|_{L^\infty(0,\infty;L^2(\Omega))}^2\right). \tag{3.11}$$

Dropping the third and fifth left hand side terms and applying Poincaré's inequality produces

$$\left(1+\left(\frac{(\delta_M/L)^3}{2R_0C_P^2}\right)\Delta t\right)\|\omega_h^{m+1}\|_{L^2}^2\leq\|\omega_h^m\|_{L^2}^2+R^*\Delta t, \tag{3.12}$$

where

$$R^*:=R_0^{-1}\left(2\mu_1C_I^2\|\omega\|_{L^\infty(0,\infty;L^2(\Omega))}^2+C_P^2\,(\delta_M/L)^{-3}\,\|F\|_{L^\infty(0,\infty;L^2(\Omega))}^2+2\mu_2C_I^2\|\psi\|_{L^\infty(0,\infty;L^2)}^2\right).$$

Invoking Lemma 2.1 gives

$$\|\omega_h^m\|_{L^2}^2\leq\left(\frac{1}{1+\lambda^*}\right)^m\|\omega_h^0\|_{L^2}^2+2R_0C_P^2\,(\delta_M/L)^{-3}\,R^*, \tag{3.13}$$

here $\lambda^*=\left(\frac{(\delta_M/L)^3}{2R_0C_P^2}\right)\Delta t$. Using the vorticity bound on the right hand side of (3.9) produces the bound on the streamfunction. □

3.1.3. Uniqueness

Lemma 3.3. *Let $\omega_h^m,\psi_h^m\in X_h$, $\omega^{m+1},\psi^{m+1}\in X$, and $F\in L^\infty(0,\infty;L^2(\Omega))$ be given. Then, if*

$$2(1+2C_P^2)<\mu_1<\frac{(\delta_M/L)^3}{4}C_I^2H^2\quad\text{and}\quad\frac{1}{2}<\mu_2<\frac{1}{4C_I^2H^2}, \tag{3.14}$$

the solution to Algorithm 3.1, $(\omega_h^{m+1},\psi_h^{m+1})\in X_h\times X_h$, is unique under the CFL type condition

$$\Delta t<\frac{h^4}{R_0C_{inv}C_\omega^2},$$

where C_ω is defined in Lemma 3.2.

Proof. Let $\omega_h^m,\psi_h^m\in X_h$, $\omega^{m+1},\psi^{m+1}\in X$, and $F\in L^\infty(0,\infty;L^2(\Omega))$ be given. Let $((\omega_h^{m+1})_1,(\psi_h^{m+1})_1)$ and $((\omega_h^{m+1})_2,(\psi_h^{m+1})_2)$ be two pairs of solutions to (3.1). Furthermore, as the following proof contains many technical details, for readability purposes, let us define $(W,P):=((\omega_h^{m+1})_1,(\psi_h^{m+1})_1)$ and $(V,Q):=((\omega_h^{m+1})_2,(\psi_h^{m+1})_2)$. Then it holds that

$$\frac{R_0}{\Delta t}\left(W-V,v_h\right)+R_0b\left(P,W,v_h\right)-R_0b\left(Q,V,v_h\right)-\left(\frac{\partial(P-Q)}{\partial x},v_h\right)$$
$$+\left(\frac{\delta_M}{L}\right)^3\left(\nabla(W-V),\nabla v_h\right)+\mu_1\left(I_H(W-V),v_h\right)=0\quad\forall\,v_h\in X_h, \tag{3.15}$$
$$\left(\nabla(P-Q),\nabla\chi_h\right)+\mu_2\left(I_H(P-Q),\chi_h\right)-\left(W-V,\chi_h\right)=0\quad\forall\,\chi_h\in X_h. \tag{3.16}$$

Taking $v_h = W - V$ in (3.15) and $\chi_h = (P-Q) - \Delta_h(P-Q)$ in (3.16), using the definition of the discrete Laplacian (2.4), and adding and subtracting appropriate terms, we have

$$\frac{R_0}{\Delta t}\|W-V\|_{L^2}^2 + R_0 b(P,W,W-V) - R_0 b(Q,V,W-V) - \left(\frac{\partial(P-Q)}{\partial x}, W-V\right) + \left(\frac{\delta_M}{L}\right)^3 \|\nabla(W-V)\|_{L^2}^2 + \mu_1\left(I_H(W-V), W-V\right) = 0,$$

$$\|\nabla(P-Q)\|_{L^2}^2 + \|\Delta_h(P-Q)\|_{L^2}^2 + \mu_2\left(I_H(P-Q), P-Q\right) + \mu_2\left(\nabla I_H(P-Q), \nabla(P-Q)\right) - (W-V, P-Q) - (\nabla(W-V), \nabla(P-Q)) = 0.$$

Multiplying both equations above by Δt, adding and subtracting appropriate terms, and adding the two equations together, we have

$$\begin{aligned}
&\left(R_0 + \mu_1\Delta t\right)\|W-V\|_{L^2}^2 + \left(\frac{\delta_M}{L}\right)^3 \Delta t\|\nabla(W-V)\|_{L^2}^2 + \mu_2\Delta t\|P-Q\|_{L^2}^2 \\
&\quad + (1+\mu_2)\Delta t\|\nabla(P-Q)\|_{L^2}^2 + \Delta t\|\Delta_h(P-Q)\|_{L^2}^2 = R_0\Delta t\, b(Q,V,W-V) \\
&\quad - R_0\Delta t\, b(P,W,W-V) + \Delta t\left(\frac{\partial(P-Q)}{\partial x}, W-V\right) + \mu_1\Delta t\left((W-V) - I_H(W-V), W-V\right) \\
&\quad + \mu_2\Delta t\left(\nabla((P-Q) - I_H(P-Q)), \nabla(P-Q)\right) + \mu_2\Delta t\left((P-Q) - I_H(P-Q), P-Q\right) \\
&\quad + \Delta t(W-V, P-Q) + \Delta t(\nabla(W-V), \nabla(P-Q)).
\end{aligned}$$

We proceed by bounding each term on the right-hand side of the equation above as follows. All estimates will use Hölder's and Young's inequalities. For the nonlinear terms, we use a standard inverse inequality, the triangle inequality, Lemmas 2.2 and 3.2, and Lemma 2 from [39] (which utilizes Ladyzhenskaya's and Poincaré's inequalities) to obtain

$$\begin{aligned}
R_0\Delta t\left(b(Q,V,W-V) - b(P,W,W-V)\right) &= \frac{R_0\Delta t}{2}\left(b(Q,V+W+V-W,W-V) - b(P,W+V+W-V,W-V)\right) \\
&= \frac{R_0\Delta t}{2}\left(b(Q,W+V,W-V) - b(P,W+V,W-V)\right) \\
&= -\frac{R_0\Delta t}{2} b(P-Q,W+V,W-V) \\
&\le \frac{R_0\Delta t}{2}\|\Delta_h(P-Q)\|_{L^2}\|\nabla(W+V)\|_{L^2}\|\nabla(W-V)\|_{L^2} \\
&\le \frac{R_0\Delta t}{2}\|\Delta_h(P-Q)\|_{L^2}\frac{C_{inv}}{h}\|W+V\|_{L^2}\|\nabla(W-V)\|_{L^2} \\
&\le \frac{R_0\Delta t}{2}\|\Delta_h(P-Q)\|_{L^2}\frac{2C_{inv}C_\omega}{h}\|\nabla(W-V)\|_{L^2} \\
&\le \frac{\Delta t}{4}\|\Delta_h(P-Q)\|_{L^2}^2 + \frac{R_0^2C_{inv}^2C_\omega^2\Delta t}{h^2}\|\nabla(W-V)\|_{L^2}^2 \\
&\le \frac{\Delta t}{4}\|\Delta_h(P-Q)\|_{L^2}^2 + \frac{R_0^2C_{inv}^4C_\omega^2\Delta t}{h^4}\|W-V\|_{L^2}^2.
\end{aligned}$$

For the third term, we have

$$\begin{aligned}
\Delta t\left(\frac{\partial(P-Q)}{\partial x}, W-V\right) &\le \Delta t\|\nabla(P-Q)\|_{L^2}\|W-V\|_{L^2} \\
&\le \frac{\Delta t}{4}\|\nabla(P-Q)\|_{L^2}^2 + \Delta t\|W-V\|_{L^2}^2.
\end{aligned}$$

For the next three terms, we implement the interpolation operator properties (2.5) and (2.6) and Young's and Poincaré's inequalities to obtain

$$\mu_1\Delta t\left((W-V) - I_H(W-V), W-V\right) \le \frac{\mu_1C_I^2H^2\Delta t}{2}\|\nabla(W-V)\|_{L^2}^2 + \frac{\mu_1\Delta t}{2}\|W-V\|_{L^2}^2,$$

$$\mu_2\Delta t\left((P-Q) - I_H(P-Q), P-Q\right) \le \frac{\mu_2C_I^2H^2\Delta t}{2}\|\nabla(P-Q)\|_{L^2}^2 + \frac{\mu_2\Delta t}{2}\|P-Q\|_{L^2}^2,$$

$$\mu_2\Delta t\left(\nabla((P-Q) - I_H(P-Q)), \nabla(P-Q)\right) \le \frac{\mu_2C_I^2H^2\Delta t}{2}\|\Delta_h(P-Q)\|_{L^2}^2 + \frac{\mu_2\Delta t}{2}\|\nabla(P-Q)\|_{L^2}^2.$$

Finally, the last two terms are treated as follows

$$\frac{\Delta t}{4}\|\nabla(P-Q)\|_{L^2}^2 \le C_P^2\Delta t\|W-V\|_{L^2}^2 + \frac{\Delta t}{4}\|\nabla(P-Q)\|_{L^2}^2,$$

and

$$\Delta t(\nabla(W-V), \nabla(P-Q)) \le \Delta t\|W-V\|_{L^2}^2 + \frac{\Delta t}{4}\|\Delta_h(P-Q)\|_{L^2}^2$$

Combining like terms, we have

$$\left(R_0 - \frac{R_0^2 C_{inv}^4 C_\omega^2 \Delta t}{h^4} + \Delta t\left(\mu_1 - 2 - C_P^2\right)\right)\|W - V\|_{L^2}^2 + \Delta t\left(\left(\frac{\delta_M}{L}\right)^3 - \frac{\mu_1 C_I^2 H^2}{2}\right)\|\nabla(W - V)\|_{L^2}^2 + \frac{\mu_2 \Delta t}{2}\|P - Q\|_{L^2}^2$$
$$+\left(\frac{1}{2} - \frac{\mu_2 C_I^2 H^2}{2} + \frac{\mu_2}{2}\right)\Delta t\|\nabla(P - Q)\|_{L^2}^2 + \Delta t\left(\frac{1}{2} - \frac{\mu_2 C_I^2 H^2}{2}\right)\|\Delta_h(P - Q)\|_{L^2}^2 \le 0.$$

Requiring the following conditions concludes the proof:

$$2(1 + 2C_P^2) \le \mu_1 \le \frac{(\delta_M/L)^3}{4C_I^2 H^2},$$
$$\mu_2 \le \frac{1}{4C_I^2 H^2},$$

and

$$\Delta t < \frac{h^4}{R_0 C_{inv}^4 C_\omega^2}. \quad \square$$

3.2. Error analysis

We now prove a long-time error bound, which is made possible by CDA.

Theorem 3.1. *Let the true solution $\psi, \omega \in L^\infty(0,\infty; H^{k+1}(\Omega) \cap H_0^1(\Omega))$, $k \ge 2$ correspond to the degree of the polynomial in the definition of Y_h, $\omega_{tt} \in L^\infty(0,\infty; L^2(\Omega))$, and $\omega_t, \omega_{tt} \in L^\infty(0,\infty; H^{k+1}(\Omega))$. Assume that Δt is sufficiently small, and that H, μ_1, and μ_2 satisfy*

$$\min\{2 + 16C_P^2,\ 4CR_0^2\left(\|\nabla\omega^{m+1}\|_{L^\infty}^2 + h^2|\omega^{m+1}|_{H^3}^2\right)\} \le \mu_1 \le \frac{(\delta_M/L)^3}{4C_I^2 H^2},$$
$$0 \le \mu_2 \le \frac{1}{4C_I^2 H^2}.$$

Then, for any time t_{m+1}, $m = 0, 1, 2, \ldots$, we have for solutions of Algorithm 3.1,

$$\|\omega^{m+1} - \omega_h^{m+1}\|_{L^2}^2 \le 2\left[\left(1 + \lambda^*\right)^{-m-1}\|\omega^0 - \omega_h^0\|_{L^2}^2 + 2R_0 C_P^2 (\delta_M/L)^{-3} R^{**} + C h^{2k+2}\|\omega\|_{L^\infty(0,\infty;H^{k+1}(\Omega))}^2\right] := C_\omega^*, \tag{3.17}$$

and

$$\|\psi^{m+1} - \psi_h^{m+1}\|_{L^2}^2 \le 2\left[C h^{2k+2}\left((2\mu_2 C_P^2 C_I^2 + 1)\|\psi\|_{L^\infty(0,\infty;H^{k+1}(\Omega))}^2 + 4C_P^4\|\omega\|_{L^\infty(0,\infty;H^{k+1}(\Omega))}^2\right) + 4C_P^4 C_\omega^*\right], \tag{3.18}$$

where $\lambda^* := \frac{(\delta_M/L)^3}{2R_0 C_P^2}\Delta t$ and

$$\begin{aligned} R^{**} :=& R_0^{-1}\Bigg[12R_0^2 C_P^2\left(\frac{\delta_M}{L}\right)^{-3} h^{2k+2}\left(\|\omega_t\|_{L^\infty(0,\infty;H^{k+1}(\Omega))}^2 + \|\omega_{tt}\|_{L^2(0,\infty;H^{k+1}(\Omega))}^2\right) \\ &+ 6C(\delta_M/L)^{-3} h^{2k+2}\|\psi\|_{L^\infty(0,\infty;H^{k+1}(\Omega))}^2 \\ &+ 2C\mu_1 C_I^2 h^{2k+2}\|\omega\|_{L^\infty(0,\infty;H^{k+1}(\Omega))}^2 + 6R_0^2 C_P^2 \Delta t^2 (\delta_M/L)^{-3}\|\omega_{tt}\|_{L^\infty(0,\infty;L^2(\Omega))}^2 \\ &+ 6CR_0^2 h^{2k+2}(\delta_M/L)^{-3}\|\nabla\omega^{m+1}\|_{L^\infty}^2\|\psi\|_{L^\infty(0,\infty;H^{k+1}(\Omega))}^2 \\ &+ 6CR_0^2 h^{4k}(\delta_M/L)^{-3}\|\psi\|_{L^\infty(0,\infty;H^{k+1}(\Omega))}^2\|\omega\|_{L^\infty(0,\infty;H^{k+1}(\Omega))}^2 \\ &+ 6CR_0^2 h^{2k+2}(\delta_M/L)^{-3}\|\nabla\psi^{m+1}\|_{L^\infty}^2\|\omega\|_{L^\infty(0,\infty;H^{k+1}(\Omega))}^2 \\ &+ Ch^{2k+2}\left[4\mu_2 C_I^2\|\psi\|_{L^\infty(0,\infty;H^{k+1}(\Omega))}^2 + 8C_P^2\|\omega\|_{L^\infty(0,\infty;H^{k+1}(\Omega))}^2\right]\Bigg]. \end{aligned}$$

Remark 3.2. *The above long-time error estimate is optimal, i.e. for m large enough,*

$$\|\omega^m - \omega_h^m\|_{L^2} + \|\psi^m - \psi_h^m\|_{L^2} \le \mathcal{O}(h^{k+1} + \Delta t).$$

Proof. The true solutions at t_{m+1} satisfy the equations: for all $v_h, \chi_h \in X_h$

$$R_0\left(\frac{\omega^{m+1} - \omega^m}{\Delta t}, v_h\right) + R_0 b(\psi^{m+1}, \omega^{m+1}, v_h) - \left(\frac{\partial\psi^{m+1}}{\partial x}, v_h\right) + \left(\frac{\delta_M}{L}\right)^3\left(\nabla\omega^{m+1}, \nabla v_h\right)$$
$$= R_0\left(\frac{\omega^{m+1} - \omega^m}{\Delta t} - \omega_t^{m+1}, v_h\right) + (F^{m+1}, v_h), \tag{3.19}$$
$$\left(\nabla\psi^{m+1}, \nabla\chi_h\right) = (\omega^{m+1}, \chi_h), \tag{3.20}$$

where $\psi^m := \psi(t_m)$ and $\omega^m := \omega(t_m)$, $m = 0, 1, 2, \ldots$. Denoting

$$\mathbb{e}^{\omega,m} := \mathbb{e}_R^{\omega,m} + \mathbb{e}_h^{\omega,m}, \quad \mathbb{e}_R^{\omega,m} := \omega^m - R_h\omega^m, \quad \mathbb{e}_h^{\omega,m} := R_h\omega^m - \omega_h^m,$$
$$\mathbb{e}^{\psi,m} := \mathbb{e}_R^{\psi,m} + \mathbb{e}_h^{\psi,m}, \quad \mathbb{e}_R^{\psi,m} := \psi^m - R_h\psi^m, \quad \mathbb{e}_h^{\psi,m} := R_h\psi^m - \psi_h^m.$$

Subtracting (3.1)-(3.2) from (3.19)-(3.20) results in

$$R_0\left(\frac{\mathbb{e}^{\omega,m+1} - \mathbb{e}^{\omega,m}}{\Delta t}, v_h\right) + R_0 b(\psi^{m+1}, \omega^{m+1}, v_h) - R_0 b(\psi_h^{m+1}, \omega_h^{m+1}, v_h) - \left(\frac{\partial \mathbb{e}^{\psi,m+1}}{\partial x}, v_h\right)$$
$$+ \left(\frac{\delta_M}{L}\right)^3 \left(\nabla \mathbb{e}^{\omega,m+1}, \nabla v_h\right) + \mu_1(I_H(\mathbb{e}^{\omega,m+1}), v_h) = R_0\left(\frac{\omega^{m+1} - \omega^m}{\Delta t} - \omega_t^{m+1}, v_h\right),$$
$$\left(\nabla \mathbb{e}^{\psi,m+1}, \nabla \chi_h\right) + \mu_2(I_H(\mathbb{e}^{\psi,m+1}), \chi_h) = (\mathbb{e}^{\omega,m+1}, \chi_h).$$

Using the error decomposition and properties of the projection R_h, setting $v_h = \mathbb{e}_h^{\omega,m+1}$ and $\chi_h = \mathbb{e}_h^{\psi,m+1}$, and applying the polarization identity produces

$$\frac{R_0}{2\Delta t}\left[\|\mathbb{e}_h^{\omega,m+1}\|_{L^2}^2 - \|\mathbb{e}_h^{\omega,m}\|_{L^2}^2 + \|\mathbb{e}_h^{\omega,m+1} - \mathbb{e}_h^{\omega,m}\|_{L^2}^2\right] + \left(\frac{\delta_M}{L}\right)^3 \|\nabla \mathbb{e}_h^{\omega,m+1}\|_{L^2}^2 + \mu_1\|\mathbb{e}_h^{\omega,m+1}\|_{L^2}^2$$
$$= -R_0\left(\frac{\mathbb{e}_R^{\omega,m+1} - \mathbb{e}_R^{\omega,m}}{\Delta t}, \mathbb{e}_h^{\omega,m+1}\right) + \left(\frac{\partial \mathbb{e}_R^{\psi,m+1}}{\partial x}, \mathbb{e}_h^{\omega,m+1}\right) + \left(\frac{\partial \mathbb{e}_h^{\psi,m+1}}{\partial x}, \mathbb{e}_h^{\omega,m+1}\right)$$
$$- \mu_1\left(I_H(\mathbb{e}_R^{\omega,m+1}), \mathbb{e}_h^{\omega,m+1}\right) - \mu_1\left(I_H(\mathbb{e}_h^{\omega,m+1}) - \mathbb{e}_h^{\omega,m+1}, \mathbb{e}_h^{\omega,m+1}\right) + R_0 b(\psi_h^{m+1}, \omega_h^{m+1}, \mathbb{e}_h^{\omega,m+1})$$
$$- R_0 b(\psi^{m+1}, \omega^{m+1}, \mathbb{e}_h^{\omega,m+1}) - R_0\left(\omega_t^{m+1} - \frac{\omega^{m+1} - \omega^n}{\Delta t}, \mathbb{e}_h^{\omega,m+1}\right), \tag{3.21}$$

and

$$\|\nabla \mathbb{e}_h^{\psi,m+1}\|_{L^2}^2 + \mu_2\|\mathbb{e}_h^{\psi,m+1}\|_{L^2}^2$$
$$= -\mu_2\left(I_H(\mathbb{e}_R^{\psi,m+1}), \mathbb{e}_h^{\psi,m+1}\right) - \mu_2\left(I_H(\mathbb{e}_h^{\psi,m+1}) - \mathbb{e}_h^{\psi,m+1}, \mathbb{e}_h^{\psi,m+1}\right) + \left(\mathbb{e}_R^{\omega,m+1}, \mathbb{e}_h^{\psi,m+1}\right) + \left(\mathbb{e}_h^{\omega,m+1}, \mathbb{e}_h^{\psi,m+1}\right). \tag{3.22}$$

Now, we bound the right hand side terms of (3.21). Applying Cauchy-Schwarz and Young's inequalities to the first term on (3.21) yields

$$R_0\left(\frac{\mathbb{e}_R^{\omega,m+1} - \mathbb{e}_R^{\omega,m}}{\Delta t}, \mathbb{e}_h^{\omega,m+1}\right) \le R_0\left\|\frac{\mathbb{e}_R^{\omega,m+1} - \mathbb{e}_R^{\omega,m}}{\Delta t}\right\|_{L^2} C_P\|\nabla \mathbb{e}_h^{\omega,m+1}\|_{L^2}$$
$$\le \frac{R_0^2 C_P^2}{2\alpha}\left(\frac{\delta_M}{L}\right)^{-3}\left\|\frac{\mathbb{e}_R^{\omega,m+1} - \mathbb{e}_R^{\omega,m}}{\Delta t}\right\|_{L^2}^2 + \frac{\alpha}{2}\left(\frac{\delta_M}{L}\right)^3\|\nabla \mathbb{e}_h^{\omega,m+1}\|_{L^2}^2, \tag{3.23}$$

and thanks to Taylor's theorem with integral remainder, some algebraic manipulations, integrating by parts, the Cauchy-Schwarz inequality, and assuming Δt is sufficiently small, we get

$$\left\|\frac{\mathbb{e}_R^{\omega,m+1} - \mathbb{e}_R^{\omega,m}}{\Delta t}\right\|_{L^2}^2 \le \int_\Omega\left(\frac{1}{\Delta t}\int_{t_m}^{t_{m+1}} (\mathbb{e}_R^\omega)_t\, dt\right)^2 d\Omega$$
$$\le \int_\Omega\left(2|(\mathbb{e}_R^\omega)_t(t_{m+1})|^2 + 2\int_{t_m}^{t_{m+1}} |(\mathbb{e}_R^\omega)_{tt}|^2 dt\right) d\Omega$$
$$\le 2\,\|(\mathbb{e}_R^\omega)_t(t_{m+1})\|_{L^2}^2 + 2\int_{t_m}^{t_{m+1}} \|(\mathbb{e}_R^\omega)_{tt}\|_{L^2}^2 dt.$$

Plugging this estimate into (3.23) produces

$$R_0\left(\frac{\mathbb{e}_R^{\omega,m+1} - \mathbb{e}_R^{\omega,m}}{\Delta t}, \mathbb{e}_h^{\omega,m+1}\right) \le \frac{R_0^2 C_P^2}{\alpha}\left(\frac{\delta_M}{L}\right)^{-3}\left(\|(\mathbb{e}_R^\omega)_t(t_{m+1})\|_{L^2}^2 + \int_{t_m}^{t_{m+1}} \|(\mathbb{e}_R^\omega)_{tt}\|_{L^2}^2 dt\right) + \frac{\alpha}{2}\left(\frac{\delta_M}{L}\right)^3\|\nabla \mathbb{e}_h^{\omega,m+1}\|_{L^2}^2.$$

The second and the third terms are estimated by using the Cauchy-Schwarz and Young's inequalities via

$$\left(\frac{\partial \mathbb{e}_R^{\psi,m+1}}{\partial x}, \mathbb{e}_h^{\omega,m+1}\right) \le \|\mathbb{e}_R^{\psi,m+1}\|_{L^2}\|\nabla \mathbb{e}_h^{\omega,m+1}\|_{L^2}^2$$
$$\le \frac{1}{2\alpha}\left(\frac{\delta_M}{L}\right)^{-3}\|\mathbb{e}_R^{\psi,m+1}\|_{L^2}^2 + \frac{\alpha}{2}\left(\frac{\delta_M}{L}\right)^3\|\nabla \mathbb{e}_h^{\omega,m+1}\|_{L^2}^2,$$

and

$$\left(\frac{\partial \mathbb{e}_h^{\psi,m+1}}{\partial x}, \mathbb{e}_h^{\omega,m+1}\right) \le \|\nabla \mathbb{e}_h^{\psi,m+1}\|_{L^2}\|\mathbb{e}_h^{\omega,m+1}\|_{L^2}$$
$$\le \frac{1}{2}\|\nabla \mathbb{e}_h^{\psi,m+1}\|_{L^2}^2 + \frac{1}{2}\|\mathbb{e}_h^{\omega,m+1}\|_{L^2}^2.$$

For the fourth and fifth terms, we use (2.5)-(2.6) together with the standard inequalities which gives

$$\begin{aligned}
\mu_1\left(I_H(\mathbb{e}_R^{\omega,m+1}), \mathbb{e}_h^{\omega,m+1}\right) &\le \mu_1 C_I \|\mathbb{e}_R^{\omega,m+1}\|_{L^2}\|\mathbb{e}_h^{\omega,m+1}\|_{L^2} \\
&\le \mu_1 C_I^2 \|\mathbb{e}_R^{\omega,m+1}\|_{L^2}^2 + \frac{\mu_1}{4}\|\mathbb{e}_h^{\omega,m+1}\|_{L^2}^2, \\
&\le \mu_1 C C_I^2 h^{2k+2}|\omega^{m+1}|_{k+1}^2 + \frac{\mu_1}{4}\|\mathbb{e}_h^{\omega,m+1}\|_{L^2}^2, \\
\mu_1\left(I_H(\mathbb{e}_h^{\omega,m+1}) - \mathbb{e}_h^{\omega,m+1}, \mathbb{e}_h^{\omega,m+1}\right) &\le \mu_1 C_I H \|\nabla \mathbb{e}_h^{\omega,m+1}\|_{L^2}\|\mathbb{e}_h^{\omega,m+1}\|_{L^2} \\
&\le \mu_1 C_I^2 H^2 \|\nabla \mathbb{e}_h^{\omega,m+1}\|_{L^2}^2 + \frac{\mu_1}{4}\|\mathbb{e}_h^{\omega,m+1}\|_{L^2}^2.
\end{aligned}$$

To estimate the skew-symmetric terms, first rewrite them as follows:

$$\begin{aligned}
R_0\left[b(\psi^{m+1}, \omega^{m+1}, \mathbb{e}_h^{\omega,m+1}) - b(\psi_h^{m+1}, \omega_h^{m+1}, \mathbb{e}_h^{\omega,m+1})\right] &= R_0\big[b(\psi^{m+1}, \omega^{m+1}, \mathbb{e}_h^{\omega,m+1}) - b(\psi_h^{m+1}, \omega_h^{m+1}, \mathbb{e}_h^{\omega,m+1}) \\
&\quad - b(\psi_h^{m+1}, \omega^{m+1}, \mathbb{e}_h^{\omega,m+1}) + b(\psi_h^{m+1}, \omega^{m+1}, \mathbb{e}_h^{\omega,m+1})\big] \\
&= R_0\left[b(\mathbb{e}^{\psi,m+1}, \omega^{m+1}, \mathbb{e}_h^{\omega,m+1}) + b(\psi_h^{m+1}, \mathbb{e}^{\omega,m+1}, \mathbb{e}_h^{\omega,m+1})\right] \\
&= R_0\left[b(\mathbb{e}^{\psi,m+1}, \omega^{m+1}, \mathbb{e}_h^{\omega,m+1}) + b(\psi_h^{m+1}, \mathbb{e}_R^{\omega,m+1}, \mathbb{e}_h^{\omega,m+1})\right] \\
&= R_0\big[b(\mathbb{e}^{\psi,m+1}, \omega^{m+1}, \mathbb{e}_h^{\omega,m+1}) + b(\psi_h^{m+1}, \mathbb{e}_R^{\omega,m+1}, \mathbb{e}_h^{\omega,m+1}) \\
&\quad - b(\psi^{m+1}, \mathbb{e}_R^{\omega,m+1}, \mathbb{e}_h^{\omega,m+1}) + b(\psi^{m+1}, \mathbb{e}_R^{\omega,m+1}, \mathbb{e}_h^{\omega,m+1})\big] \\
&= R_0[b(\mathbb{e}^{\psi,m+1}, \omega^{m+1}, \mathbb{e}_h^{\omega,m+1}) + b(\psi^{m+1}, \mathbb{e}_R^{\omega,m+1}, \mathbb{e}_h^{\omega,m+1}) - b(\mathbb{e}^{\psi,m+1}, \mathbb{e}_R^{\omega,m+1}, \mathbb{e}_h^{\omega,m+1})] \\
&= R_0[\,b(\mathbb{e}_R^{\psi,m+1}, \omega^{m+1}, \mathbb{e}_h^{\omega,m+1}) - b(\mathbb{e}_h^{\psi,m+1}, \omega^{m+1}, \mathbb{e}_h^{\omega,m+1}) + b(\psi^{m+1}, \mathbb{e}_R^{\omega,m+1}, \mathbb{e}_h^{\omega,m+1}) \\
&\quad - b(\mathbb{e}_R^{\psi,m+1}, \mathbb{e}_R^{\omega,m+1}, \mathbb{e}_h^{\omega,m+1}) + b(\mathbb{e}_h^{\psi,m+1}, \mathbb{e}_R^{\omega,m+1}, \mathbb{e}_h^{\omega,m+1})].
\end{aligned}$$

Applying Hölder and Young inequalities along with approximation properties, the first two skew-symmetric terms can be bounded as

$$\begin{aligned}
R_0\, b(\mathbb{e}_R^{\psi,m+1}, \omega^{m+1}, \mathbb{e}_h^{\omega,m+1}) &\le R_0 C \|\mathbb{e}_R^{\psi,m+1}\|_{L^2}\|\nabla\omega^{m+1}\|_{L^\infty}\|\nabla \mathbb{e}_h^{\omega,m+1}\|_{L^2} \\
&\le \frac{R_0^2 C\, h^{2k+2}}{2\alpha}\left(\frac{\delta_M}{L}\right)^{-3}\|\nabla\omega^{m+1}\|_{L^\infty}^2|\psi^{m+1}|_{k+1}^2 + \frac{\alpha}{2}\left(\frac{\delta_M}{L}\right)^{3}\|\nabla \mathbb{e}_h^{\omega,m+1}\|_{L^2}^2,
\end{aligned}$$

and

$$\begin{aligned}
R_0 b(\mathbb{e}_h^{\psi,m+1}, \omega^{m+1}, \mathbb{e}_h^{\omega,m+1}) &\le R_0 C \|\nabla \mathbb{e}_h^{\psi,m+1}\|_{L^2}\|\nabla\omega^{m+1}\|_{L^\infty}\|\mathbb{e}_h^{\omega,m+1}\|_{L^2} \\
&\le \frac{R_0^2 C}{2\alpha^*}\|\nabla\omega^{m+1}\|_{L^\infty}^2\|\mathbb{e}_h^{\omega,m+1}\|_{L^2}^2 + \frac{\alpha^*}{2}\|\nabla \mathbb{e}_h^{\psi,m+1}\|_{L^2}^2.
\end{aligned}$$

Now, the inverse inequality together with Hölder's and Young's inequalities give that

$$\begin{aligned}
R_0 b(\psi^{m+1}, \mathbb{e}_R^{\omega,m+1}, \mathbb{e}_h^{\omega,m+1}) &\le R_0 C \|\nabla\psi^{m+1}\|_{L^\infty}\|\mathbb{e}_R^{\omega,m+1}\|_{L^2}\|\nabla \mathbb{e}_h^{\omega,m+1}\|_{L^2} \\
&\le R_0 C \|\nabla\psi^{m+1}\|_{L^\infty} h^{k+1}|\,\omega^{m+1}|_{k+1}\|\nabla \mathbb{e}_h^{\omega,m+1}\|_{L^2} \\
&\le \frac{R_0^2 C h^{2k+2}}{2\alpha}\left(\frac{\delta_M}{L}\right)^{-3}\|\nabla\psi^{m+1}\|_{L^\infty}^2|\omega^{m+1}|_{k+1}^2 + \frac{\alpha}{2}\left(\frac{\delta_M}{L}\right)^{3}\|\nabla \mathbb{e}_h^{\omega,m+1}\|_{L^2}^2,
\end{aligned}$$

and

$$\begin{aligned}
R_0 b(\mathbb{e}_R^{\psi,m+1}, \mathbb{e}_R^{\omega,m+1}, \mathbb{e}_h^{\omega,m+1}) &\le R_0 C \|\mathbb{e}_R^{\psi,m+1}\|\|\nabla \mathbb{e}_R^{\omega,m+1}\|_{H^1}\|\nabla \mathbb{e}_h^{\omega,m+1}\|_{L^2} \\
&\le R_0 C \|\mathbb{e}_R^{\psi,m+1}\|h^{-1}\|\nabla \mathbb{e}_R^{\omega,m+1}\|_{L^2}\|\nabla \mathbb{e}_h^{\omega,m+1}\|_{L^2} \\
&\le R_0 C h^{k+1}|\,\psi^{m+1}|_{k+1} h^{k-1}|\omega^{m+1}|_{k+1}\|\nabla \mathbb{e}_h^{\omega,m+1}\|_{L^2} \\
&\le \frac{R_0^2 C h^{4k}}{2\alpha}\left(\frac{\delta_M}{L}\right)^{-3}|\psi^{m+1}|_{k+1}^2|\omega^{m+1}|_{k+1}^2 + \frac{\alpha}{2}\left(\frac{\delta_M}{L}\right)^{3}\|\nabla \mathbb{e}_h^{\omega,m+1}\|_{L^2}^2,
\end{aligned}$$

and

$$R_0 b(\mathbb{e}_h^{\psi,m+1}, \mathbb{e}_R^{\omega,m+1}, \mathbb{e}_h^{\omega,m+1}) \le R_0 C \|\nabla \mathbb{e}_h^{\psi,m+1}\|_{L^2} \|\nabla \mathbb{e}_R^{\omega,m+1}\|_{L^\infty} \|\mathbb{e}_h^{\omega,m+1}\|_{L^2}$$
$$\le \frac{R_0^2 C}{2\alpha^*} \|\nabla \mathbb{e}_R^{\omega,m+1}\|_{L^\infty}^2 \|\mathbb{e}_h^{\omega,m+1}\|_{L^2}^2 + \frac{\alpha^*}{2} \|\nabla \mathbb{e}_h^{\psi,m+1}\|_{L^2}^2.$$

For the last term, first, apply Taylor's theorem and then use Cauchy-Schwarz and Young's inequalities to get

$$R_0 \left(\omega_t^{m+1} - \frac{\omega^{m+1} - \omega^m}{\Delta t}, \mathbb{e}_h^{\omega,m+1} \right) \le R_0 (\Delta t/2) \|\omega_{tt}(t_*)\|_{L^2} C_P \|\nabla \mathbb{e}_h^{\omega,m+1}\|_{L^2}$$
$$\le \frac{R_0^2 C_P^2 \Delta t^2}{8\alpha} \left(\frac{\delta_M}{L} \right)^{-3} \|\omega_{tt}(t_*)\|_{L^2}^2 + \frac{\alpha}{2} \left(\frac{\delta_M}{L} \right)^3 \|\nabla \mathbb{e}_h^{\omega,m+1}\|_{L^2}^2,$$

where $t_* \in [t_m, t_{m+1}]$. Choosing $\alpha^* = 1/2$, $\alpha = 1/6$, substituting all these estimates to the right hand side of (3.21), combining like terms and using approximating properties produces

$$\frac{R_0}{2\Delta t} \left[\|\mathbb{e}_h^{\omega,m+1}\|_{L^2}^2 - \|\mathbb{e}_h^{\omega,m}\|_{L^2}^2 + \|\mathbb{e}_h^{\omega,m+1} - \mathbb{e}_h^{\omega,m}\|_{L^2}^2 \right] + \frac{1}{2} \left[\mu_1 - \left(1 + 2R_0^2 C \left[\|\nabla \omega^{m+1}\|_{L^\infty}^2 + \|\nabla \mathbb{e}_R^{\omega,m+1}\|_{L^\infty}^2 \right] \right) \right] \|\mathbb{e}_h^{\omega,m+1}\|_{L^2}^2$$
$$+ \frac{1}{2} \left(\frac{\delta_M}{L} \right)^3 \left[1 - 2\mu_1 C_I^2 H^2 (\delta_M/L)^{-3} \right] \|\nabla \mathbb{e}_h^{\omega,m+1}\|_{L^2}^2$$
$$\le 6R_0^2 C_P^2 \left(\frac{\delta_M}{L} \right)^{-3} \left(\|(\mathbb{e}_R^\omega)_t(t_{m+1})\|_{L^2}^2 + \int_{t_m}^{t_{m+1}} \|(\mathbb{e}_R^\omega)_{tt}\|_{L^2}^2 dt \right) + 3C (\delta_M/L)^{-3} h^{2k+2} |\psi^{m+1}|_{k+1}^2$$
$$+ C\mu_1 C_I^2 h^{2k+2} |\omega^{m+1}|_{k+1}^2 + (3/4) R_0^2 C_P^2 \Delta t^2 (\delta_M/L)^{-3} \|\omega_{tt}(t^*)\|_{L^2}^2 + 3C R_0^2 h^{2k+2} (\delta_M/L)^{-3} \|\nabla \omega^{m+1}\|_{L^\infty}^2 |\psi^{m+1}|_{k+1}^2$$
$$+ 3C R_0^2 h^{4k} (\delta_M/L)^{-3} |\psi^{m+1}|_{k+1}^2 |\omega^{m+1}|_{k+1}^2 + 3C R_0^2 h^{2k+2} (\delta_M/L)^{-3} \|\nabla \psi^{m+1}\|_{L^\infty}^2 |\omega^{m+1}|_{k+1}^2 + \|\nabla \mathbb{e}_h^{\psi,m+1}\|_{L^2}^2. \tag{3.24}$$

Proceeding similarly, we are able to bound the right-hand side of equation (3.22) as follows

$$\|\nabla \mathbb{e}_h^{\psi,m+1}\|_{L^2}^2 + \mu_2 \|\mathbb{e}_h^{\psi,m+1}\|_{L^2}^2 = \mu_2 \left(I_H(\mathbb{e}_R^{\psi,m+1}), \mathbb{e}_h^{\psi,m+1} \right) - \mu_2 \left(I_H(\mathbb{e}_h^{\psi,m+1}) - \mathbb{e}_h^{\psi,m+1}, \mathbb{e}_h^{\psi,m+1} \right)$$
$$+ \left(\mathbb{e}_R^{\omega,m+1}, \mathbb{e}_h^{\psi,m+1} \right) - \left(\mathbb{e}_h^{\omega,m+1}, \mathbb{e}_h^{\psi,m+1} \right)$$
$$\le \mu_2 C_I \|\mathbb{e}_R^{\psi,m+1}\|_{L^2} \|\mathbb{e}_h^{\psi,m+1}\|_{L^2} + \mu_2 C_I H \|\nabla \mathbb{e}_h^{\psi,m+1}\|_{L^2} \|\mathbb{e}_h^{\psi,m+1}\|_{L^2}$$
$$+ \|\mathbb{e}_R^{\omega,m+1}\|_{L^2} C_P \|\nabla \mathbb{e}_h^{\psi,m+1}\|_{L^2} + \|\mathbb{e}_h^{\omega,m+1}\|_{L^2} C_P \|\nabla \mathbb{e}_h^{\psi,m+1}\|_{L^2}.$$
$$\le \frac{\mu_2 C_I^2}{2} \|\mathbb{e}_R^{\psi,m+1}\|_{L^2}^2 + \frac{\mu_2}{2} \|\mathbb{e}_h^{\psi,m+1}\|_{L^2}^2 + \mu_2 C_I^2 H^2 \|\nabla \mathbb{e}_h^{\psi,m+1}\|^2 + \frac{\mu_2}{4} \|\mathbb{e}_h^{\psi,m+1}\|_{L^2}^2$$
$$+ C_P^2 \|\mathbb{e}_R^{\omega,m+1}\|^2 + \frac{1}{4} \|\nabla \mathbb{e}_h^{\psi,m+1}\|^2 + C_P^2 \|\mathbb{e}_h^{\omega,m+1}\|^2 + \frac{1}{4} \|\nabla \mathbb{e}_h^{\psi,m+1}\|_{L^2}^2.$$

Rearranging terms together with the use of the approximation properties on the right hand side results in

$$\frac{1}{2} \left(1 - 2\mu_2 C_I^2 H^2 \right) \|\nabla \mathbb{e}_h^{\psi,m+1}\|_{L^2}^2 + \frac{\mu_2}{4} \|\mathbb{e}_h^{\psi,m+1}\|_{L^2}^2 \le C h^{2k+2} \left[(\mu_2 C_I^2)/2 |\psi^{m+1}|_{k+1}^2 + C_P^2 |\omega^{m+1}|_{k+1}^2 \right] + C_P^2 \|\mathbb{e}_h^{\omega,m+1}\|_{L^2}^2.$$

Under the assumption that H is sufficiently small and μ_2 is sufficiently large, multiplying the inequality above by 4 and dropping the second left hand side term yields

$$\|\nabla \mathbb{e}_h^{\psi,m+1}\|_{L^2}^2 \le C h^{2k+2} \left[2\mu_2 C_I^2 |\psi^{m+1}|_{k+1}^2 + 4C_P^2 |\omega^{m+1}|_{k+1}^2 \right] + 4C_P^2 \|\mathbb{e}_h^{\omega,m+1}\|_{L^2}^2. \tag{3.25}$$

Substituting this into (3.24) produces

$$\frac{R_0}{2\Delta t} \left[\|\mathbb{e}_h^{\omega,m+1}\|_{L^2}^2 - \|\mathbb{e}_h^{\omega,n}\|_{L^2}^2 + \|\mathbb{e}_h^{\omega,m+1} - \mathbb{e}_h^{\omega,m}\|_{L^2}^2 \right] + \frac{1}{2} \left[\mu_1 - \left[1 + 8 C_P^2 + 2R_0^2 C \left(\|\nabla \omega^{m+1}\|_{L^\infty}^2 + \|\nabla \mathbb{e}_R^{\omega,m+1}\|_{L^\infty}^2 \right) \right] \right] \|\mathbb{e}_h^{\omega,m+1}\|_{L^2}^2$$
$$+ \frac{1}{2} \left(\frac{\delta_M}{L} \right)^3 \left[1 - 2\mu_1 C_I^2 H^2 \left(\frac{\delta_M}{L} \right)^{-3} \right] \|\mathbb{e}_h^{\omega,m+1}\|_{L^2}^2$$
$$\le 6R_0^2 C_P^2 \left(\frac{\delta_M}{L} \right)^{-3} \left(\|(\mathbb{e}_R^\omega)_t(t_{m+1})\|^2 + \int_{t_m}^{t_{m+1}} \|(\mathbb{e}_R^\omega)_{tt}\|^2 dt \right) + 3C (\delta_M/L)^{-3} h^{2k+2} |\psi^{m+1}|_{k+1}^2$$
$$+ C\mu_1 C_I^2 h^{2k+2} |\omega^{m+1}|_{k+1}^2 + (3/4) R_0^2 C_P^2 \Delta t^2 (\delta_M/L)^{-3} \|\omega_{tt}(t_*)\|_{L^2}^2 + 3C R_0^2 h^{2k+2} (\delta_M/L)^{-3} \|\nabla \omega^{m+1}\|_{L^\infty}^2 |\psi^{m+1}|_{k+1}^2$$
$$+ 3C R_0^2 h^{4k} (\delta_M/L)^{-3} |\psi^{m+1}|_{k+1}^2 |\omega^{m+1}|_{k+1}^2 + 3C R_0^2 h^{2k+2} (\delta_M/L)^{-3} \|\nabla \psi^{m+1}\|_{L^\infty}^2 |\omega^{m+1}|_{k+1}^2 + C h^{2k+2} \left[2\mu_2 C_I^2 |\psi^{m+1}|_{k+1}^2 + 4C_P^2 |\omega^{m+1}|_{k+1}^2 \right].$$

First, use the assumption of the lemma, divide by $\frac{R_0}{2\Delta t}$, drop the third and the fourth left hand side terms. Then applying the Poincaré's inequality to the fifth term on the left hand side yields

$$\left(1 + \left(\frac{(\delta_M/L)^3}{2R_0 C_P^2} \right) \Delta t \right) \|\mathbb{e}_h^{\omega,m+1}\|_{L^2}^2 \le \|\mathbb{e}_h^{\omega,m}\|_{L^2}^2 + R_0^{-1} \left[12R_0^2 C_P^2 \left(\frac{\delta_M}{L} \right)^{-3} h^{2k+2} \left(\|\omega_t(t_{m+1})\|_{L^2}^2 + \|\omega_{tt}\|_{L^2(t_m, t_{m+1}; L^2)}^2 \right) \right.$$
$$\left. + 6C (\delta_M/L)^{-3} h^{2k+2} |\psi^{m+1}|_{k+1}^2 + 2C\mu_1 C_I^2 h^{2k+2} |\omega^{m+1}|_{k+1}^2 + (3/2) R_0^2 C_P^2 \Delta t^2 (\delta_M/L)^{-3} \|\omega_{tt}(t^*)\|_{L^2}^2 \right.$$

$$+ 6\,C\,R_0^2 h^{2k+2}\,(\delta_M/L)^{-3}\,\|\nabla\omega^{m+1}\|_{L^\infty}^2 |\psi^{m+1}|_{k+1}^2 + 6\,C\,R_0^2 h^{4k}\,(\delta_M/L)^{-3}\,|\psi^{m+1}|_{k+1}^2 |\omega^{m+1}|_{k+1}^2$$
$$+ 6\,C\,R_0^2 h^{2k+2}\,(\delta_M/L)^{-3}\,\|\nabla\psi^{m+1}\|_{L^\infty}^2 |\omega^{m+1}|_{k+1}^2 + C\,h^{2k+2}(4\mu_2 C_I^2 |\psi^{m+1}|_{k+1}^2 + 8C_P^2 |\omega^{m+1}|_{k+1}^2)\Big]\Delta t.$$

Rearranging terms yields

$$\left(1+\left(\frac{(\delta_M/L)^3}{2R_0C_P^2}\right)\Delta t\right)\|\mathfrak{e}_h^{\omega,m+1}\|_{L^2}^2 \le \|\mathfrak{e}_h^{\omega,m}\|_{L^2}^2 \;+\; R^{**}\Delta t,$$

where

$$\begin{aligned}
R^{**} :=& R_0^{-1}\Big[12R_0^2C_P^2\left(\frac{\delta_M}{L}\right)^{-3}h^{2k+2}\left(\|\omega_t\|^2_{L^\infty(0,\infty;H^{k+1}(\Omega))}+\|\omega_{tt}\|^2_{L^2(0,\infty;H^{k+1}(\Omega))}\right)\\
&+\;6C\,(\delta_M/L)^{-3}\,h^{2k+2}\|\psi\|^2_{L^\infty(0,\infty;H^{k+1}(\Omega))}\\
&+\;2C\,\mu_1C_I^2h^{2k+2}\|\omega\|^2_{L^\infty(0,\infty;H^{k+1}(\Omega))}+\;6\,R_0^2C_P^2\Delta t^2\,(\delta_M/L)^{-3}\,\|\omega_{tt}\|^2_{L^\infty(0,\infty;L^2(\Omega))}\\
&+\;6\,C\,R_0^2h^{2k+2}\,(\delta_M/L)^{-3}\,\|\nabla\omega^{m+1}\|^2_{L^\infty}\|\psi\|^2_{L^\infty(0,\infty;H^{k+1}(\Omega))}\\
&+\;6\,C\,R_0^2h^{4k}\,(\delta_M/L)^{-3}\,\|\psi\|^2_{L^\infty(0,\infty;H^{k+1}(\Omega))}\|\omega\|^2_{L^\infty(0,\infty;H^{k+1}(\Omega))}\\
&+\;6\,C\,R_0^2h^{2k+2}\,(\delta_M/L)^{-3}\,\|\nabla\psi^{m+1}\|^2_{L^\infty}\|\omega\|^2_{L^\infty(0,\infty;H^{k+1}(\Omega))}\\
&+\;Ch^{2k+2}\left[4\mu_2C_I^2\,\|\psi\|^2_{L^\infty(0,\infty;H^{k+1}(\Omega))}+8C_P^2\,\|\omega\|^2_{L^\infty(0,\infty;H^{k+1}(\Omega))}\right]\Big].
\end{aligned}$$

Invoking Lemma 2.1 yields

$$\|\mathfrak{e}_h^{\omega,m+1}\|_{L^2}^2 \le \left(\frac{1}{1+\left(\frac{(\delta_M/L)^3}{2R_0C_P^2}\right)\Delta t}\right)^{m+1}\|\mathfrak{e}_h^{\omega,0}\|_{L^2}^2 \;+\; 2\,R_0C_P^2\,(\delta_M/L)^{-3}R^{**} =: C_\omega, \tag{3.26}$$

then applying the triangle inequality gives (3.17). To get (3.18), first apply Poincare's inequality to obtain $\|\mathfrak{e}_h^{\psi,m+1}\|_{L^2}^2 \le C_P^2\|\nabla\mathfrak{e}_h^{\psi,m+1}\|_{L^2}^2$ and use this in (3.25). Applying the triangle inequality together with (3.17) finishes the proof. □

4. Numerical experiments

In this section, we test the numerical scheme presented and analyzed above. Additionally, since the scheme above (for simplicity) uses backward Euler time stepping, we also test its BDF2 analogue, which is given by Algorithm (4.1) below. Generally speaking, BDF2 analogues of backward Euler methods have very similar properties in terms of stability, but BDF2 temporal discretizations are typically second order while backward Euler temporal discretization are first order. The analysis usually follows a similar pattern provided G-stability theory is used, although with more technical details, see e.g. [2,30,44]. Hence we expect the BDF2 algorithm to behave very similarly to backward Euler but with greater temporal accuracy.

Algorithm 4.1 *(BDF2-CDA algorithm). Let $\omega^{m+1} := \omega(t_{m+1})$ and $\psi^{m+1} := \psi(t_{m+1})$ be the solution to the BV system (1.1) at time t_{m+1} and let the forcing term at time t_{m+1}, denoted by $F^{m+1} := F(t_{m+1})$, be given. Given $\omega_h^0, \omega_h^1 \in X_h$, find $\omega_h^{m+1} \in X_h$ and $\psi_h^{m+1} \in X_h$, for $m = 1, 2, 3, \ldots$ satisfying*

$$R_0\left(\frac{3\omega_h^{m+1}-4\omega_h^m+\omega_h^{m-1}}{2\Delta t},v_h\right)+R_0b(\psi_h^{m+1},\omega_h^{m+1},v_h)-\left(\frac{\partial\psi_h^{m+1}}{\partial x},v_h\right)$$
$$+\left(\frac{\delta_M}{L}\right)^3\left(\nabla\omega_h^{m+1},\nabla v_h\right)+\mu_1(I_H(\omega_h^{m+1}-\omega^{m+1}),v_h)=(F^{m+1},v_h), \tag{4.1}$$
$$\left(\nabla\psi_h^{m+1},\nabla\chi_h\right)+\mu_2(I_H(\psi_h^{m+1}-\psi^{m+1}),\chi_h)=(\omega_h^{m+1},\chi_h), \tag{4.2}$$

for every $v_h, \chi_h \in X_h$.

For all of our tests, we use $P_2(\tau_h)$ approximations for X_h, and enforce Dirichlet boundary condition on all boundaries. We also use $Y_H = P_0(\tau_H)$, where τ_H is a coarse mesh approximation of Ω with $h \le H$. For the interpolant, we choose $I_H = P_{Y_H}^{L^2}$, i.e. the L^2 projection operator onto Y_H. This is known to satisfy the required properties (2.5) and (2.6) [45].

4.1. Convergence rate verification

To illustrate the spatial and temporal convergence rates (and verify our codes), we pick a time dependent analytical solution on $\Omega = (0,1)\times(-1,1)$ to be

$$\omega := 2\pi^2\exp\left[-\frac{2\pi^2}{R_0}\left(\frac{\delta_M}{L}\right)^3 t\right]\sin(\pi x)\sin(\pi y),$$

Table 1
Spatial vorticity and streamfunction errors and rates for BE-CDA with $R_0 = 1.0$, $\frac{\delta_M}{L} = 0.7$, $\mu_1 = 100 = \mu_2$. Rate approximations are calculated by: rate $\approx \frac{\ln(err_{j-1}/err_j)}{\ln 2}$.

h	$\|\omega(T) - \omega_h^M\|_{L^2}$	Rate	$\|\psi(T) - \psi_h^M\|_{L^2}$	Rate
1/2	5.3359e-2	–	2.8786e-3	–
1/4	7.9584e-3	2.7452	4.1730e-4	2.7862
1/8	1.0850e-3	2.8748	5.5679e-5	2.9059
1/16	1.4227e-4	2.9310	7.0840e-6	2.9745
1/32	1.9680e-5	2.8538	9.3061e-7	2.9283

Table 2
Spatial vorticity and streamfunction errors and rates for BDF2-CDA with $R_0 = 1.0$, $\frac{\delta_M}{L} = 0.7$, $\mu_1 = 100 = \mu_2$. Rate approximations are calculated by rate $\approx \frac{\ln(err_{j-1}/err_j)}{\ln 2}$.

h	$\|\omega(T) - \omega_h^M\|_{L^2}$	Rate	$\|\psi(T) - \psi_h^M\|_{L^2}$	Rate
1/2	1.7008e-4	–	9.1115e-6	–
1/4	2.5435e-5	2.7414	1.3182e-6	2.7891
1/8	3.4449e-6	2.8842	1.7564e-7	2.9079
1/16	4.4131e-7	2.9646	2.2373e-8	2.9727
1/32	5.6113e-8	2.9754	2.8129e-9	2.9916

Table 3
Temporal vorticity and streamfunction errors and rates for BE-CDA with $R_0 = 1.0$, $\frac{\delta_M}{L} = 0.7$, $\mu_1 = 100 = \mu_2$. Rate approximations are calculated by rate $\approx \frac{\ln(err_{j-1}/err_j)}{\ln 2}$.

Δt	$\|\omega(T) - \omega_h^M\|_{L^2}$	Rate	$\|\psi(T) - \psi_h^M\|_{L^2}$	Rate
1/2	2.3891e-2	–	1.9968e-4	–
1/4	1.1275e-2	1.0833	9.4222e-5	1.0835
1/8	5.0312e-3	1.1642	4.2034e-5	1.1645
1/16	2.3792e-3	1.0804	1.9877e-5	1.0805
1/32	1.1575e-3	1.0395	9.6848e-6	1.0373
1/64	5.7093e-4	1.0196	4.8228e-6	1.0059

$$\psi := \exp\left[-\frac{2\pi^2}{R_0}\left(\frac{\delta_M}{L}\right)^3 t\right]\sin(\pi x)\sin(\pi y).$$

From these solutions, we calculate the forcing term from (1.1) to be

$$F := -\pi \exp\left[-\frac{2\pi^2}{R_0}\left(\frac{\delta_M}{L}\right)^3 t\right]\cos(\pi x)\sin(\pi y).$$

We enforce Dirichlet boundary condition nodally on all of Ω for both the streamfunction and vorticity, choose $R_0 = 1$, $\frac{\delta_M}{L} = 0.7$ for backward Euler and BDF2, impose zero initial condition for the vorticity and streamfunction, use $H = h$, and set $\mu_1 = \mu_2 = 100$. An end time of $T = 1$ is used for all the convergence rate tests.

We begin with the spatial convergence rates, and use errors from successively refined meshes with mesh width h to approximate the exponent in: error $\sim O(h^{rate})$. To isolate the spatial error, we take the time step size to be $\Delta t = 0.001$, and vary only the mesh width size h. The results are given in Table 1 for backward Euler and in Table 2 for BDF2. In both cases, we observe the spatial convergence rates for both the vorticity and streamfunction to be third order in the L^2 norm, which is optimal and in agreement with our analysis since P_2 elements are used.

To isolate the temporal errors, in order to approximate the temporal convergence rate from: error $\sim \Delta t^{rate}$, we fix $h = 1/32$ and the end time $T = 1.0$, and vary Δt. The results are shown in Table 3 for backward Euler and Table 4 for BDF2, and we observed first and second order convergence respectively, which are both optimal and in agreement with our analysis.

4.2. Double gyre wind forcing experiment

We now test the proposed method on the benchmark double gyre wind forcing test. This problem is used to model ocean dynamics in several studies, in particular as a benchmark test to analyze new techniques for turbulent geophysical flows [40,28,47,39]. When the BV system is forced by a double gyre wind forcing in a rectangular basin and the dissipation is weak, the instantaneous fields of vorticity and streamfunction are highly variable. However, the mean fields show a well defined four gyre pattern in which the two central gyres are driven by the wind with its

Table 4
Temporal vorticity and streamfunction errors and rates for BDF2-CDA with $R_0 = 1.0$, $\frac{\delta_M}{L} = 0.7$, $\mu_1 = 100 = \mu_2$. Rate approximations are calculated by rate $\approx \frac{\ln(err_{j-1}/err_j)}{\ln 2}$.

Δt	$\|\omega(T) - \omega_h^M\|_{L^2}$	Rate	$\|\psi(T) - \psi_h^M\|_{L^2}$	Rate
1/4	1.1579e-3	—	9.6724e-6	—
1/8	2.0375e-4	2.5070	1.7020e-6	2.5067
1/16	3.7789e-5	2.4307	3.1567e-7	2.4307
1/32	7.7320e-6	2.2891	6.4594e-8	2.2890
1/64	1.7503e-6	2.1433	1.4630e-8	2.1425
1/128	4.1666e-7	2.0707	3.5000e-9	2.0635
1/256	9.5780e-8	2.1211	8.6453e-10	2.0174

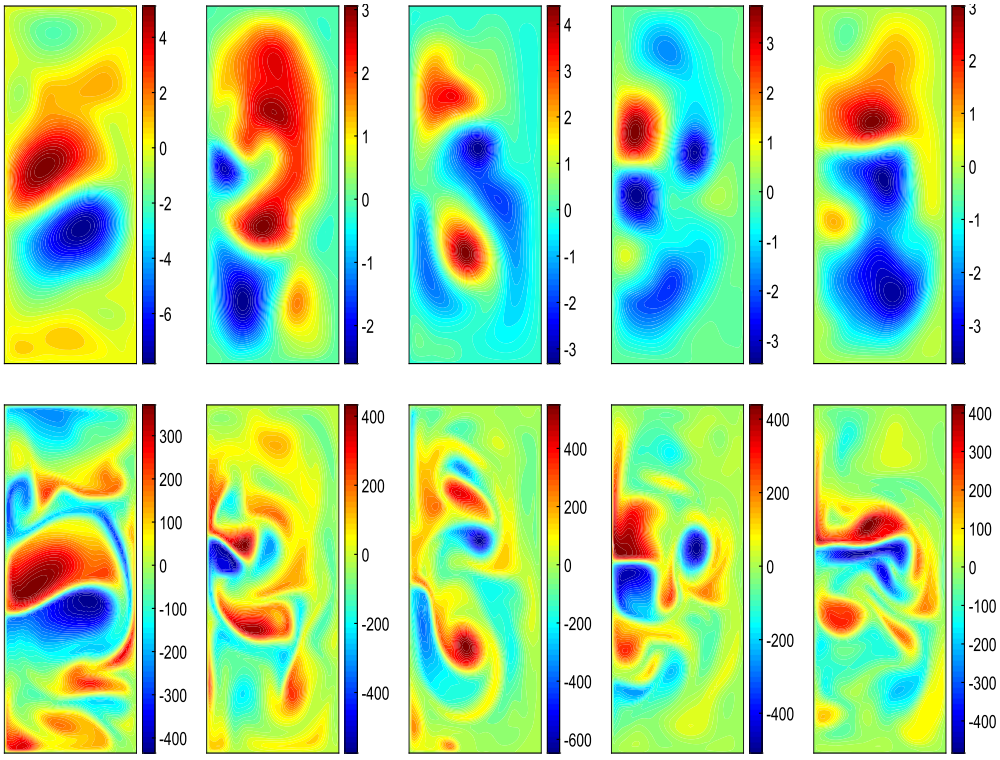

Fig. 1. Shown above are contour plots of streamfunction (top) and vorticity (bottom) with $Ro = 0.0016$ for the BV model in the double gyre wind forcing test, at times t = 2,4,8,16,24 (left to right).

same orientation, and the southern and northern ends of the basin circulate in the opposite direction, driven by the eddy flux of potential vorticity [25,28].

This problem has the following setup [47]. The domain is set as $\Omega = (0,1) \times (-1,1)$, the forcing is $F = \sin(\pi y)$, ${}^{\delta_M}/_{L} = 0.02$, and $Ro = 0.0016$ (which corresponds to $Re = 200$). Plots of the streamfunction and vorticity at times t = 2,4,8,16,24 are shown in Fig. 1, and we observe a very complex flow from these snapshots in time.

For this test, we restrict to only the BDF2-CDA algorithm. As we do not have a true analytical solution, we first generate a solution (called the true solution below) using P_2 elements on a mesh created as a 25×50 uniform triangulation that is refined again around the top, bottom and left edges and then refined once more along the left edge (providing approximately 20 K total degrees of freedom). The time step size was chosen to be $\Delta t = 0.004$, and the solution was computed up to $T = 24$, starting from an initial condition of 0 and using the BDF2-CDA algorithm but not with CDA, i.e. we set $\mu_1 = \mu_2 = 0$.

We next computed the BDF2-CDA algorithm on the same mesh and time step size, using an initial condition of 0 for both the streamfunction and the vorticity, starting the simulation from t = 4 (the CDA solution at time t is nudged towards the $t + 4$ true solution). We run several tests here, the first with $H = h$ (as many measurement points as possible) so that we can observe the best that BDF2-CDA can perform and also test different choices of μ_1 and μ_2. We then test with large μ_1 and μ_2, and with varying H to observe how large H can be and still get convergence. We note that the use of large parameters is not common in CDA methods, and the ability to take such large parameters is thanks (at least in part) to the use of implicit time stepping.

For the tests with $H = h$, we computed with varying $\mu_1 = \mu_2$, and the plots of the difference between the BDF2-CDA solution and the true solution are shown in Fig. 2. We observe rapid convergence of the CDA solution to the true solution for $\mu_1 = \mu_2 \geq 0.1$, and even faster convergence as the nudging parameter is increased. However, with nudging too small, i.e. $\mu_1 = \mu_2 = 0.01$, no convergence is observed. We note that since the

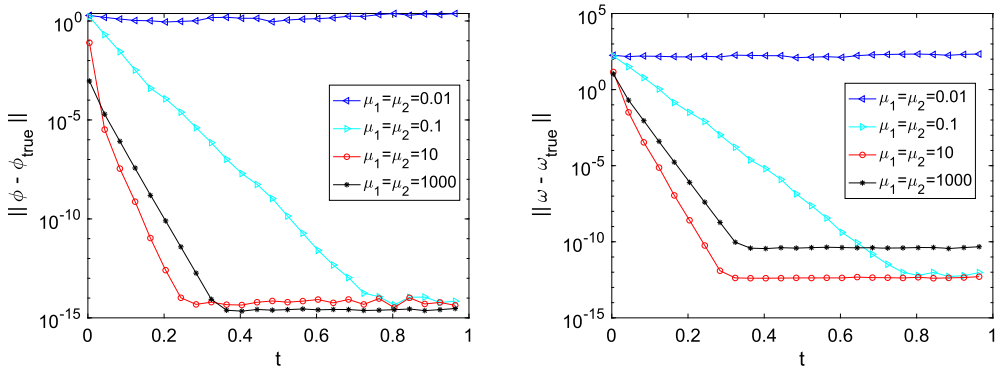

Fig. 2. Shown above are the L^2 differences between the true and CDA streamfunctions (left) and vorticities (right), where both vorticity and the streamfunction are nudged.

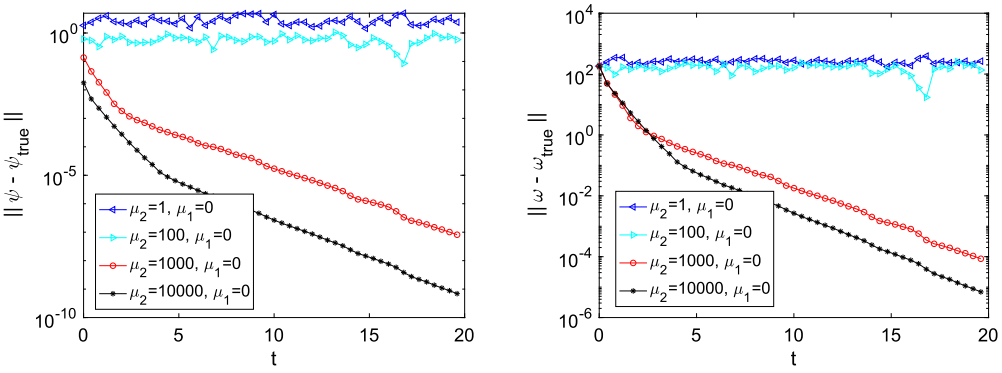

Fig. 3. Shown above are the L^2 differences between the true and CDA streamfunctions (left) and vorticities (right), where only the streamfunction is nudged.

true solution comes from a computation on the same mesh as the CDA, convergence goes down to near the level of roundoff error (instead of to a level near $O(h^3 + \Delta t^2)$. It is interesting that the results with $\mu_1 = \mu_2 = 10$ are slightly better than with $\mu_1 = \mu_2 = 1000$. This is consistent with our analysis, since the error bounds in Theorem 3.1 contain the nudging parameters in the upper bounds on the error. This suggests there may be optimal positive nudging parameters, but an analysis sharper than what we have given may be necessary to determine such parameters.

Next, we repeat the same test but only nudge the streamfunction, i.e. we take $\mu_1 = 0$, since in practice accurately measuring vorticity can be difficult. We note the above analysis does not apply to this case, since the analysis assumes μ_1 is positive and sufficiently large. However, there is evidence at least for Rayleigh-Bénard systems that nudging all unknowns in CDA applications may not be necessary [15,1], and so it is worth testing this case. We observe from Fig. 3 that for $\mu_2 \geq 1000$, convergence of the CDA solution to the true solution is still achieved, although it takes much longer to converge compared to when vorticity is also nudged. With $\mu_2 \leq 100$, however, no convergence is achieved. For this case, we see overall improvement as μ_2 is increased from 1 to 10,000. However, since this is outside the scope of our analysis, it is unclear why this is the case (comparing to when $\mu_1 = \mu_2$ when nudging parameters of 10 are better than 1000). The analysis of a new CDA scheme in which only the streamfunction is nudged is currently under investigation and reserved for future work.

Lastly, we consider the case of less measurement data and large nudging parameters. Since we saw no deterioration of accuracy in our tests for $\mu_1 = \mu_2 = 10000$ (shown above) and even larger (tests omitted) nudging parameters, we consider now the limit of very large nudging parameters. Despite our analysis having sufficient conditions that nudging parameters not be too large, our numerical tests suggest the analysis may be improvable and the upper bound on nudging parameters may be removed as in [20] for specific interpolants and formulation (including those used herein). Numerically, when algebraic nudging is used for I_H [45], the implementation of CDA reduces to simply enforcing that the BDF2-CDA solutions take the value of the true solution at specific nodes directly (i.e. directly in the linear system), so the idea of very large nudging parameters is very interesting from an implementation viewpoint. We note that large nudging parameters were considered for Navier-Stokes equations in [41,42,27,33]; while these were in a somewhat different setting, they showed that the general idea of large nudging or direct enforcement toward data can be effective. We considered the same double gyre forcing test as above but now with N =200, 150, 100 and 50 total measurement points, chosen at random from the fine mesh nodes, where the true solution streamfunction and vorticity are nudged. Convergence results are shown in Fig. 4, as the difference between the BDF2-CDA solution and the true solution in L^2, and we observe that with 200 measurement points convergence is achieved, although not monotonically. For N =150, we do not get obvious convergence but the L^2 error has an overall decreasing (but erratic) trend. When N =100 or 50 measurement points are used, no convergence is observed. Based on the success of these tests, the authors believe the analysis above can be extended to the case of larger H and nudging parameters, and plan to consider this in future work.

The tests above for the benchmark double gyre wind forcing experiment were repeated with the forcing changed from $\sin(\pi y)$ to $\sin(\pi y) + \sin(2\pi y)$. The reason for this modification is that $\sin(\pi y)$ is an eigenfunction of the Laplacian, and in some related equations if the forcing is such an eigenfunction then it can lead to uninteresting long-time behavior. Our test results for this modified forcing were qualitatively similar to that of the benchmark problem, and so we omitted the results.

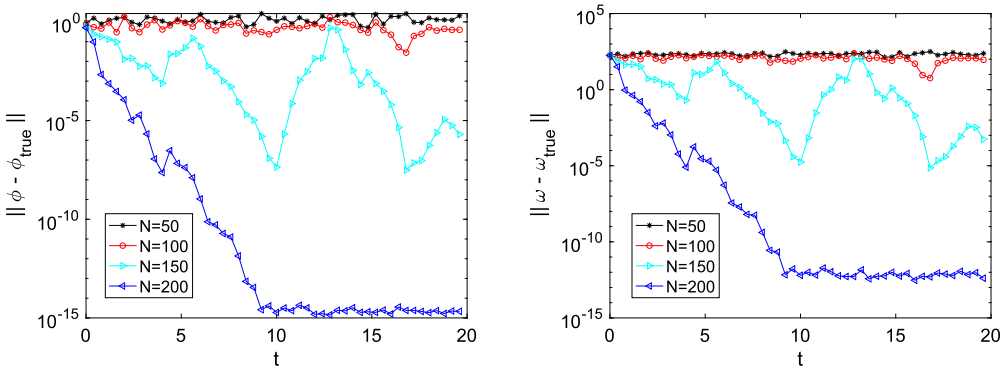

Fig. 4. Shown above are the L^2 differences between the true and CDA streamfunctions (left) and vorticities (right), with varying number of measurement data points.

5. Conclusions

We studied herein a CDA algorithm for the discretized BV system. We proved that for parameters chosen in a range determined by our analysis, long-time stability of the L^2 vorticity and H^1 streamfunction is achieved. Numerical results illustrated the theory, both with predicted convergence rates and also with showing the effectiveness of the method on an application problem.

For future work, we plan to consider similar methods that do not nudge the vorticity. Measuring vorticity in practice can be difficult, and thus nudging only the streamfunction would be more practical. The method studied herein was tested numerically without vorticity nudging and it seemed to work, although not nearly as well as when vorticity nudging was used. Our analysis, however, does require vorticity nudging, and thus either an improved analysis for a modified algorithm will need constructed.

Data availability

Data will be made available on request.

References

[1] L. Agasthy, P.C. Di Leoni, L. Biferale, Reconstructing Rayleigh-Bénard flows out of temperature-only measurements using nudging, Phys. Fluids 34 (1) (2022).
[2] M. Akbas, S. Kaya, L. Rebholz, On the stability at all times of linearly extrapolated BDF2 timestepping for multiphysics incompressible flow problems, Numer. Methods Partial Differ. Equ. 33 (4) (2017) 995–1017.
[3] M.U. Altaf, E.S. Titi, T. Gebrael, O.M. Knio, L. Zhao, M.F. McCabe, I. Hoteit, Downscaling the 2D Bénard convection equations using continuous data assimilation, Comput. Geosci. 21 (2017) 393–410.
[4] A. Azouani, E. Olson, E.S. Titi, Continuous data assimilation using general interpolant observables, J. Nonlinear Sci. 24 (2014) 277–304.
[5] V. Barcilon, P. Constantin, E. Titi, Existence of solutions to the Stommel-Charney model of the Gulf Stream, SIAM J. Math. Anal. 19 (6) (1988) 1355–1364.
[6] A. Biswas, K.R. Brown, V.R. Martinez, Mesh-free interpolant observables for continuous data assimilation, Ann. Appl. Math. 38 (2022) 296–355.
[7] S.C. Brenner, L.R. Scott, The Mathematical Theory of Finite Element Methods, Texts in Applied Mathematics, vol. 15, Springer Science+Business Media, LLC, 2008.
[8] D. Bresch, D. Gérard-Varet, Roughness-induced effects on the quasi-geostrophic model, Commun. Math. Phys. 253 (1) (2005) 81–119.
[9] E. Carlson, J. Hudson, A. Larios, Parameter recovery for the 2 dimensional Navier-Stokes equations via continuous data assimilation, SIAM J. Sci. Comput. 42 (1) (2020) A250–A270.
[10] E. Carlson, J. Hudson, A. Larios, V.R. Martinez, E. Ng, J.P. Whitehead, Dynamically learning the parameters of a chaotic system using partial observations, Discrete Contin. Dyn. Syst. 42 (8) (2022) 3809–3839.
[11] E. Carlson, A. Larios, Sensitivity analysis for the 2D Navier–Stokes equations with applications to continuous data assimilation, J. Nonlinear Sci. 31 (84) (2021).
[12] A.E. Diegel, L.G. Rebholz, Continuous data assimilation and long-time accuracy in a C^0 interior penalty method for the Cahn-Hilliard equation, Appl. Math. Comput. 424 (2022) 127042.
[13] G. Evensen, Sequential data assimilation with a nonlinear quasi-geostrophic model using Monte Carlo methods to forecast error statistics, J. Geophys. Res. 99 (1994) 10.
[14] A. Farhat, N.E. Glatt-Holtz, V.R. Martinez, S.A. McQuarrie, J.P. Whitehead, Data assimilation in large Prandtl Rayleigh-Bénard convection from thermal measurements, SIAM J. Appl. Dyn. Syst. 19 (1) (2020) 510–540.
[15] A. Farhat, H. Johnston, M. Jolly, E. Titi, Assimilation of nearly turbulent Rayleigh-Bénard flow through vorticity or local circulation measurements: a computational study, J. Sci. Comput. 77 (3) (2018) 1519–1533.
[16] A. Farhat, M.S. Jolly, E.S. Titi, Continuous data assimilation for the 2D Bénard convection through velocity measurements alone, Phys. D: Nonlinear Phenom. 303 (2015) 59–66.
[17] A. Farhat, E. Lunasin, E.S. Titi, On the Charney conjecture of data assimilation employing temperature measurements alone: the paradigm of 3D planetary geostrophic model, Math. Clim. Weather Forecast. 2 (1) (2016).
[18] A. Farhat, E. Lunasin, E.S. Titi, A data assimilation algorithm: the paradigm of the 3D Leray-α model of turbulence, Part. Diff. Eq. Aris. Phys. Geom. 450 (2019) 253–273.
[19] G.J. Fix, Finite element models for ocean circulation problems, SIAM J. Appl. Math. 29 (3) (1975) 371–387.
[20] B. Garcia-Archilla, J. Novo, Error analysis of fully discrete mixed finite element data assimilation schemes for the Navier-Stokes equations, Adv. Comput. Math. (2020) 46–61.
[21] B. Garcia-Archilla, J. Novo, E. Titi, Uniform in time error estimates for a finite element method applied to a downscaling data assimilation algorithm, SIAM J. Numer. Anal. 58 (2020) 410–429.
[22] V. Girault, R.H. Nochetto, L.R. Scott, Max-norm estimates for Stokes and Navier–Stokes approximations in convex polyhedra, Numer. Math. 131 (4) (2015) 771–822.
[23] V. Girault, P.-A. Raviart, Finite Element Methods for Navier–Stokes Equations: Theory and Algorithms, Springer-Verlag, 1986.
[24] H. Goosse, H. Renssen, A. Timmermann, R.S. Bradley, Internal and forced climate variability during the last millennium: a model-data comparison using ensemble simulations, Quat. Sci. Rev. 24 (12) (2005) 1345–1360.
[25] R.J. Greatbatch, B.T. Nadiga, Four-gyre circulation in a barotropic model with double-gyre wind forcing, J. Phys. Oceanogr. 30 (6) (2000) 1461–1471.
[26] E. Hairer, G. Wanner, Solving ordinary differential equations. II, in: Stiff and Differential-Algebraic Problems, second edition, in: Springer Series in Computational Mathematics, vol. 14, Springer-Verlag, Berlin, 1996.
[27] K. Hayden, E.J. Olson, E.S. Titi, Discrete data assimilation in the Lorenz and 2D Navier-Stokes equations, Phys. D: Nonlinear Phenom. 240 (18) (2011) 1416–1420.
[28] D.D. Holm, B.T. Nadiga, Modeling mesoscale turbulence in the barotropic double-gyre circulation, J. Phys. Oceanogr. 33 (11) (2003) 2355–2365.
[29] A.H. Ibdah, C.F. Mondaini, E.S. Titi, Fully discrete numerical schemes of a data assimilation algorithm: uniform-in-time error estimates, IMA J. Numer. Anal. 40 (4) (2019) 2584–2625.

[30] N. Jiang, M. Mohebujjaman, L. Rebholz, C. Trenchea, An optimally accurate discrete regularization for second order timestepping methods for Navier-Stokes equations, Comput. Methods Appl. Mech. Eng. 310 (2016) 388–405.
[31] M.S. Jolly, V.R. Martinez, E.J. Olson, E.S. Titi, Continuous data assimilation with blurred-in-time measurements of the surface quasi-geostrophic equation, Chin. Ann. Math., Ser. B 40 (5) (2019) 721–764.
[32] M.S. Jolly, V.R. Martinez, E.S. Titi, A data assimilation algorithm for the subcritical surface quasi-geostrophic equation, Adv. Nonlinear Stud. 17 (1) (2017) 167–192.
[33] A. Larios, L.G. Rebholz, C. Zerfas, Global in time stability and accuracy of IMEX-FEM data assimilation schemes for Navier–Stokes equations, Comput. Methods Appl. Mech. Eng. 345 (2019) 1077–1093.
[34] P.C. Di Leoni, A. Mazzino, L. Biferale, Inferring flow parameters and turbulent configuration with physics-informed data assimilation and spectral nudging, Phys. Rev. Fluids 3 (104604) (2018).
[35] P.C. Di Leoni, A. Mazzino, L. Biferale, Synchronization to big data: nudging the Navier-Stokes equations for data assimilation of turbulent flows, Phys. Rev. X 10 (011023) (2020).
[36] A.J. Majda, C. Franzke, D. Crommelin, Normal forms for reduced stochastic climate models, Proc. Natl. Acad. Sci. 106 (10) (2009) 3649–3653.
[37] V.R. Martinez, Convergence analysis of a viscosity parameter recovery algorithm for the 2D Navier-Stokes equations, Nonlinearity 35 (2022) 2241–2287.
[38] T.T. Medjo, Numerical simulations of a two-layer quasi-geostrophic equation of the ocean, SIAM J. Numer. Anal. 37 (6) (2000) 2005–2022.
[39] I. Monteiro, C. Manica, L. Rebholz, Numerical study of a regularized barotropic vorticity model of geophysical flow, Numer. Methods Partial Differ. Equ. 31 (5) (2015) 1492–1514.
[40] B.T. Nadiga, L.G. Margolin, Dispersive-dissipative eddy parameterization in a barotropic model, J. Phys. Oceanogr. 31 (8) (2001) 2525–2531.
[41] E.J. Olson, E.S. Titi, Determining modes for continuous data assimilation in 2D turbulence, J. Stat. Phys. 113 (516) (2003) 799–840.
[42] E.J. Olson, E.S. Titi, Determining modes and Grashoff number for continuous data assimilation in 2D turbulence, Theor. Comput. Fluid Dyn. 22 (2008) 327–339.
[43] B. Pachev, J.P. Whitehead, S.A. McQuarrie, Concurrent MultiParameter learning demonstrated on the Kuramoto- Sivashinsky equation, SIAM J. Sci. Comput. 44 (5) (2022) A2974–A2990.
[44] L. Rebholz, F. Tone, Long-time H^1-stability of BDF2 time stepping for 2D Navier-Stokes equations, Appl. Math. Lett. 141 (108624) (2023).
[45] L.G. Rebholz, C. Zerfas, Simple and efficient continuous data assimilation of evolution equations via algebraic nudging, Numer. Methods Partial Differ. Equ. 37 (3) (2021) 2588–2612.
[46] H. Renssen, V. Brovkin, T. Fichefet, H. Goosse, Simulation of the Holocene climate evolution in Northern Africa: the termination of the African Humid Period, Quat. Int. 150 (1) (2006) 95–102.
[47] O. San, A.E. Staples, Z. Wang, T. Iliescu, Approximate deconvolution large eddy simulation of a barotropic ocean circulation model, Ocean Model. 40 (2) (2011) 120–132.
[48] G. Sutyrin, X. Carton, Vortex interaction with a zonal Rossby wave in a Quasi-Geostrophic model, Dyn. Atmos. Ocean. 41 (2) (2006) 85–102.
[49] S.-C. Yang, M. Corazza, A. Carrassi, E. Kalnay, T. Miyoshi, Comparison of ensemble-based and variational-based data assimilation schemes in a Quasi-Geostrophic model, in: AMS 10th Symposium on Integrated Observing and Assimilation Systems for the Atmosphere, Oceans, and Land Surface, 2007.